

Thermal Kinetic Inductance Detectors for Millimeter-Wave Detection

A. Wandui,^{1, a)} J.J. Bock,^{1, b)} C. Frez,² M. Hollister,³ L. Minutolo,¹ H. Nguyen,² B. Steinbach,¹ A. Turner,² J. Zmuidzinas,¹ and R. O'Brient^{2, c)}

¹⁾*Department of Physics, California Institute of Technology, Pasadena, CA, 91125, USA*

²⁾*Jet Propulsion Lab, Pasadena, CA, 91109, USA*

³⁾*Fermilab, Batavia, IL, 60510, USA*

(Dated: 31 July 2020)

Thermal Kinetic Inductance Detectors (TKIDs) combine the excellent noise performance of traditional bolometers with a radio frequency (RF) multiplexing architecture that enables the large detector counts needed for the next generation of millimeter-wave instruments. In this paper, we first discuss the expected noise sources in TKIDs and derive the limits where the phonon noise contribution dominates over the other detector noise terms: generation-recombination, amplifier, and two-level system (TLS) noise. Second, we characterize aluminum TKIDs in a dark environment. We present measurements of TKID resonators with quality factors of about 10^5 at 80 mK. We also discuss the bolometer thermal conductance, heat capacity, and time constants. These were measured by the use of a resistor on the thermal island to excite the bolometers. These dark aluminum TKIDs demonstrate a noise equivalent power $NEP = 2 \times 10^{-17} \text{W}/\sqrt{\text{Hz}}$ with a $1/f$ knee at 0.1 Hz, which provides background noise limited performance for ground based telescopes observing at 150 GHz.

I. INTRODUCTION

Cryogenic bolometers and calorimeters have found widespread use in a wide range of scientific applications including dark-matter searches¹⁻⁴ and neutrino detection⁵⁻⁷, thermal remote imaging and security cameras^{8,9}; and astronomy with wavelengths ranging from millimeter waves to gamma rays¹⁰⁻¹⁹. Modern bolometric and calorimetric instruments use Transition Edge Sensors (TESes)²⁰ for their thermometers because they can be fabricated using thin-film lithography and thus integrated into monolithic arrays with large detector counts. In practice, in order to limit the thermal cable load on the cryogenic stages, which have limited cooling capacity, multiple TESes are read out on a single line using Superconducting Quantum Interference Devices (SQUIDs)²¹. SQUIDs are low noise and have low impedance as well as sufficient bandwidth to multiplex many TESes on a single line with minimal crosstalk. The two main schemes developed to multiplex TES pixels are time-division multiplexing (TDM)^{22,23} and frequency-division multiplexing (FDM)²⁴. Currently operating instruments fielding kilo-pixel detector arrays have implemented TDM and FDM readout schemes^{10-13,25}.

The next generation of cryogenic instruments under development will require even higher detector counts^{26,27}. This is especially true for applications in which the detectors are designed to be background noise limited. In this case, gains in instrument sensitivity can only be achieved by increasing the number of detectors. However, it is challenging and expensive to integrate and read out arrays with detector counts above $\sim 10,000$ using the existing SQUID-based multiplexing schemes.

Kinetic Inductance Detectors (KIDs)²⁸⁻³⁶ are an alternative detector technology that offer a promising solution to the problem of scaling up to larger detector counts. Like TESes, KIDs can be fabricated on silicon wafers using thin-film lithography. However, each KID pixel, which is a superconducting resonator, has a unique frequency and a narrow bandwidth. This is an advantage of KIDs over TESes because large numbers of KIDs can be read out on a single transmission line using microwave frequency-division multiplexing (mFDM) without requiring complex SQUID-based readout and assembly.

In the place of SQUIDs, KID readout systems typically use fast FPGA-based^{33,37-39} or GPU-based^{40,41} digital electronic systems to generate probe tones that are sent down a coaxial line with filters and attenuators to excite the KID array. The detector responses are then amplified using a cryogenic Low Noise Amplifier (LNA) before passing out of the cryostat where they are demodulated and digitized into detector timestreams⁴².

Thermal Kinetic Inductance Detectors (TKIDs) are a variation of Kinetic Inductance Detectors and as such, they offer the same multiplexing benefits. A TKID integrates a superconducting resonator into a bolometer. Rather than tracking the changes in the resistance of the superconductor as TES bolometers do, the temperature variations of the thermally isolated island are measured by the changes in the kinetic inductance of the superconducting resonator circuit. Because all the power is thermalized on the bolometer island, a TKID's absorber can be electrically decoupled from the resonator circuit, unlike in most KID designs. This gives TKIDs an additional degree of engineering flexibility since the resonator and the absorber can be optimized independently.

TKIDs have been an active area of research since Sauvageau's⁴³ early work on kinetic inductance thermometry. TKIDs have been developed as energy detectors for X-ray imaging spectroscopy⁴⁴ to simultaneously achieve high spatial and energy resolution and for thermal X-ray photon detection⁴⁵. TKIDs have also been used as THz radiation detectors⁴⁶⁻⁴⁹ operating at kelvin-range temperatures. How-

^{a)}Electronic mail: awandui@caltech.edu.

^{b)}Also at Jet Propulsion Lab, Pasadena, CA, 91109, USA

^{c)}Also at Department of Physics, California Institute of Technology, Pasadena, CA, 91125, USA

ever, TKIDs have not yet been demonstrated as power detectors for millimeter-wave instruments that operate at sub-kelvin temperatures.

The measurement of the polarization anisotropies of the Cosmic Microwave Background (CMB) is one of the most important use cases for bolometric power detectors working in the millimeter-wave regime. CMB observations have strict requirements on detector sensitivity, stability, and scalability, especially for future experiments targeting high detector counts^{27,50}.

This paper therefore describes the performance of dark prototype devices that demonstrate the feasibility of using TKIDs for CMB observations. Our TKID design targets the detector performance requirements needed for CMB observations at 150 GHz. The devices discussed in this paper are an improvement on our initial design⁵¹ and demonstrate noise performance appropriate for background-limited ground-based CMB measurements at 150 GHz.

II. DEVICE DESIGN AND EXPECTED PERFORMANCE

Like all bolometers, TKIDs consists of a thermally isolated island on which absorbed optical power P_{opt} is converted to heat. The absorbed power causes the island temperature T to rise above the temperature of the heat sink held at a temperature T_{bath} . The thermal island has a heat capacity $C(T)$ and is attached to the heat sink via a weak link with a thermal conductance $G(T)$. The temperature gradient across the thermal link creates a net power flow P_{leg} through the weak thermal link from the island to the heat sink.

The readout circuit of a TKID consists of a parallel LC resonator built up of lumped element components. A large capacitor C sets the resonance frequency f_r , and smaller additional capacitors C_c couple the resonator to both the microstrip transmission line and to ground. The inductor, which acts as the thermometer, is on the island. The total inductance L has a geometric inductance L_g due to the shape of the inductor wire and a kinetic inductance L_k from its superconductivity.

The kinetic inductance of a superconducting film with thickness t , length l and width w , for a total volume $V_{sc} = l \cdot w \cdot t$ can be determined from the normal sheet resistance R_s of the film and its superconductor gap energy Δ using the relation $L_k = (l/w) \cdot L_s$ where $L_s = \hbar R_s / \pi \Delta$. This equation also defines the surface kinetic inductance L_s that is often specified when doing electromagnetic simulations of superconducting resonators. The gap energy is in turn determined by the superconducting transition temperature T_c via $\Delta = 1.763 k_B T_c$. Changes in L_k with temperature shift both the resonance frequency and the internal quality factor Q_i of the resonator. A large kinetic inductance fraction, $\alpha_k = L_k / (L_g + L_k)$ gives a large responsivity to thermal fluctuations⁵². This is achievable by either minimizing the geometric inductance by design, or alternatively by choosing a material with a large resistivity or a large T_c .

The bolometer also includes an absorber element on the island that receives incident radiative (optical) power. In our dark device design, we use a Au resistor R_h which can be bi-

ased through an external circuit to simulate optical loading on the island. The absorber is in thermal contact with but electrically isolated from the inductor. With this design, the absorber can be modified with no impact on the resonator. Because of this, a TKID can be used as a drop-in replacement for a TES in a bolometer in order to take advantage of already developed radiation-coupling technologies such as planar phased-array antennas, horns or lenslets^{12,13,53}. Figure 1a shows a schematic of the thermal and electrical circuit of a TKID pixel as an aid to the discussion presented here.

In the rest of this section, we build up the device model of a TKID bolometer in order to make predictions of their expected performance and noise properties. Our goal is to quantify the possible sources of noise that arise in addition to photon noise during observations. We expect detector noise contributions from 4 sources: phonon noise, generation-recombination (gr) noise, amplifier noise and two-level system (TLS) noise. Each of these noise terms is well covered in existing literature^{52,54,55} and we will therefore focus mainly on the conditions under which the total detector noise is dominated by the phonon noise which is still smaller than the expected photon noise level. Lindeman⁵⁶ also gives a discussion of the noise sources in a resonator bolometer under a bolometer matrix formalism.

A. Thermal Architecture

Bolometer theory is well established^{54,57,58} and we apply it to inform our predictions of TKID performance. There are a few notable distinctions between the operation of TKIDs and the more familiar TES bolometers that we will draw attention to.

Ignoring the noise terms at present, the thermal response of a TKID bolometer is governed by the differential equation:

$$C \frac{dT}{dt} = -P_{\text{leg}} + P_{\text{read}} + P_{\text{opt}}, \quad (1)$$

where P_{read} is the readout power dissipated by the inductor. Although the inductor is superconducting, it has a non-zero AC resistance. The net heat flow through the thermal link is modelled as $P_{\text{leg}} = K (T^n - T_{\text{bath}}^n)$, with K a coefficient, and n the power-law index. The thermal conductance of the thermal link is the derivative of P_{leg} with respect to the island temperature, $G(T) = n K T^{n-1}$. P_{read} is further discussed under section II B on the electrical properties of the bolometer.

Unlike TES bolometers, we operate TKIDs in the regime where $P_{\text{read}} \ll P_{\text{opt}}$, and therefore with negligible electro-thermal feedback. The equilibrium condition, $P_{\text{opt}} = P_{\text{leg}}$ sets the operating temperature T_o at a given bath temperature. We target a 380 mK operating temperature from a 250 mK bath temperature, accessible with a ³He cooler. Importantly, the island temperature sets the quality factor of the resonators and in turn the number of resonators that can be packed in a given readout bandwidth.

The CMB signal of interest can be described as small fluctuations in the optical power δP_{opt} . We therefore expand equa-

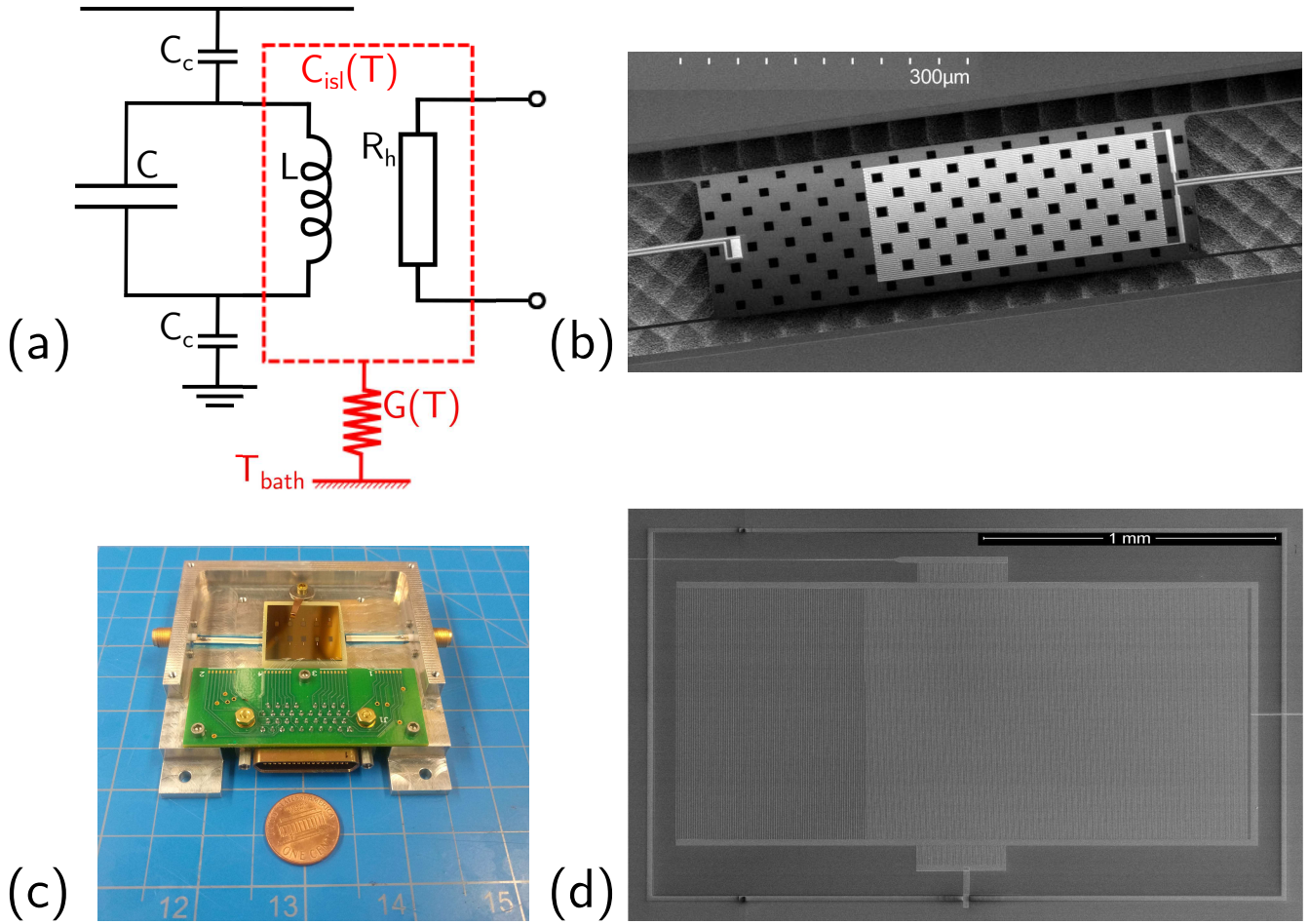


FIG. 1. (a) Schematic of a TKID bolometer. The thermal circuit is shown in red while the electrical system is depicted in black. R_h represents an Au resistor where we can deposit electrical power to simulate optical loading and to directly measure the power-to-frequency responsivity. (b) SEM micrograph of a released bolometer showing the inductor on the right and the Au heater on the left. The square holes on the island are used in the XeF_2 release process. (c) Photograph of a single TKID prototype chip with the bias circuit. (d) SEM micrograph of the TKID capacitor and coupling capacitors with a section of the feedline visible.

tion 1 to obtain the small signal response to small perturbations δT about the operating temperature. The resulting equation in Fourier space is:

$$\delta T(\nu) = \frac{\delta P_{\text{opt}}}{G(T_o)} \cdot \frac{1}{1 + j2\pi\nu\tau_{\text{bolo}}}. \quad (2)$$

Here, $G(T_o)$ is the thermal conductance at operating temperature and is determined by considering the total optical loading. The total optical loading on the detector has contributions from both the microwave emission from the sky and that of the telescope itself. The internal loading from the telescope is usually minimized by design but is often still significant. As a reference, we chose the representative measured optical loading, $P_{\text{opt}} = 4.7\text{ pW}$ of the BICEP2 telescope which observed the CMB at 150 GHz from the South Pole⁵⁹. A 4.7 pW loading requires a thermal conductance $G(T_o) \sim 55\text{ pW/K}$. This conductance is realizable using silicon nitride films with a suitable geometry⁵³. Silicon nitride films can be used to achieve thermal conductances as low as the 10 pW/K range

to match a wide range of optical loading levels. Even lower thermal conductances down to 0.1 pW/K can be achieved by incorporating phononic thermal filters in the thermal link design⁶⁰. TKID bolometers can therefore be implemented under a wide range of potential loading conditions.

The bolometer time constant, $\tau_{\text{bolo}} = C(T_o)/G(T_o)$, sets the bandwidth of the device. The device bandwidth, $\nu_{\text{BW}} = 1/(2\pi\tau_{\text{bolo}})$ must be much larger than the science frequency band, i.e. $\nu_{\text{BW}} > \dot{\theta}/\theta_{\text{FWHM}}$ where $\dot{\theta}$ is the scan rate of the telescope and θ_{FWHM} is the beam size. τ_{bolo} is expected to be on the order of a few milliseconds, setting the device bandwidth at tens of Hz, which is fast enough for ground-based degree scale CMB observations. At fixed $G(T_o)$, the device bandwidth can be increased by modifying the island design to reduce the heat capacity.

We can now consider the thermal phonon noise which is generated by the random nature of the energy transport across the bolometer thermal link. The phonon noise level, expressed as a noise equivalent power is set by the thermal conductance $G(T_o)$ as:

$$\text{NEP}_{\text{ph}}^2 = 4F(T_o, T_{\text{bath}})k_B T_o^2 G(T_o), \quad (3)$$

where the factor $F(T_o, T_{\text{bath}})$ accounts for the temperature gradient across the bolometer legs^{20,54,55}.

In comparison, the photon noise $\text{NEP}_{\text{photon}}$ for a single-mode detector in the limit where the optical bandwidth Δv_{opt} is much smaller than the optical frequency v_{opt} is given by⁶¹

$$\text{NEP}_{\text{photon}}^2 = 2h v_{\text{opt}} P_{\text{opt}} + 2 \frac{P_{\text{opt}}^2}{\Delta v_{\text{opt}}}. \quad (4)$$

To directly compare phonon noise to photon noise, we rewrite the phonon NEP by taking advantage of the fact that $P_{\text{leg}} = P_{\text{opt}}$ to eliminate $G(T_o)$ in favor of P_{opt} . We find that $\text{NEP}_{\text{ph}}^2 = 4\tilde{F}(T_o, T_{\text{bath}})k_B T_o P_{\text{opt}}$, where $\tilde{F}(T_o, T_{\text{bath}}) = F(T_o, T_{\text{bath}}) \cdot n / (1 - (T_{\text{bath}}/T_o)^n)$. For our device parameters, $F(T_o, T_{\text{bath}}) = 0.57$ and $\tilde{F}(T_o, T_{\text{bath}}) = 2.4$, giving $\text{NEP}_{\text{ph}} = 16 \text{ aW}/\sqrt{\text{Hz}}$, which is much smaller than $\text{NEP}_{\text{photon}} = 45 \text{ aW}/\sqrt{\text{Hz}}$ at $v_{\text{opt}} = 150 \text{ GHz}$, $\Delta v_{\text{opt}}/v_{\text{opt}} = 0.25$. We stress that our device is designed so that phonon noise sets the detector noise limit at operating temperature rather than other noise sources such as quasiparticle generation-recombination noise as in KIDs⁵².

B. Electrical Properties

The temperature fluctuations of the bolometer island must be converted into electrical signals that can be readout. The small signal changes in the island temperature are read out by monitoring the forward transmission S_{21} of the TKID resonator. At a readout frequency f that is close to the resonance frequency f_r , $S_{21}(f)$ for a single-pole resonator is well described using the equation^{62,63}:

$$S_{21}(f) = 1 - \frac{Q_r}{Q_c} \frac{1}{1 + j2Q_r x}, \quad (5)$$

where $x = (f - f_r)/f_r$ is the fractional detuning of the probe signal away from the resonance frequency, Q_r is the loaded resonator quality factor and Q_c is the coupling quality factor. Given Q_c and Q_i , $Q_r^{-1} = Q_i^{-1} + Q_c^{-1}$. Q_i accounts for all loss mechanism intrinsic to the resonator while Q_c is a measure of how strongly the resonator is coupled to the external circuit through the feedline and ground. Under optimal coupling, $Q_i = Q_c \implies Q_r = Q_i/2$.

Changes in the island temperature $\delta T(t)$ induce fractional changes in the resonance frequency, $\delta x = (f_r(t) - f_r)/f_r$ as well as in the resonator dissipation, $\delta_i = Q_i^{-1}(t) - Q_i^{-1}$. If these fluctuations are slower than the resonator bandwidth $f_r/2Q_r$, we are in the adiabatic limit and the response of the resonator $\delta S_{21}(v)$ at Fourier frequency v is given by

$$\delta S_{21}(v) = \frac{Q_i}{4} \chi_c \chi_g e^{-2j\phi_g} [\delta_i(v) + j2\delta x(v)], \quad (6)$$

where we have defined the coupling efficiency, $\chi_c \equiv \frac{4Q_r^2}{Q_r Q_c}$ such that $\chi_c = 1$ at optimal coupling. In addition, we also define the detuning efficiency $\chi_g \equiv [1 + 4Q_r^2 x^2]^{-1}$ with $\tan \phi_g = 2Q_r x$. Similarly, at zero detuning, $f = f_r \implies \phi_g = 0$ and $\chi_g = 1$. These quantities relate the probe signal power P_g to the power dissipated by the resonator P_{read} as $P_{\text{read}} = \frac{1}{2} \cdot \chi_c \cdot \chi_g \cdot P_g$. At optimal coupling and zero detuning, half the input power is dissipated by the resonator⁵². In the TKID case, only a portion of the resonator is on the thermal island, so the derived expression for P_{read} is an upper limit on the readout power contribution to the total loading on the island.

We can compute δx and δ_i by considering the electrodynamics of Bardeen-Cooper-Schrieffer (BCS) superconductors⁶⁴. Typically, we make the approximation that the superconductor state is fully specified once the quasiparticle density n_{qp} is known. The quasiparticle generation mechanism is a key distinction between standard KIDs and TKIDs. In KIDs, energy is injected into the quasiparticles directly via photons whereas in TKIDs, thermal phonons are the main quasiparticle generators. For aluminum TKIDs, the expected quasiparticle lifetime τ_{qp} is in the tens to hundreds of microseconds range; much smaller than the thermal time constant. Since we take the thermal quasiparticle generation to be the dominant mechanism, the total quasiparticle density reduces to the thermal quasiparticle density n_{th} given by BCS theory as⁶⁴:

$$n_{\text{th}} = 2N_0 \sqrt{2\pi k_B T \Delta} \cdot \exp \left[-\frac{\Delta}{k_B T} \right]. \quad (7)$$

As expected, n_{th} depends on the temperature T , the gap energy Δ and the single-spin density of states at the Fermi level N_0 . Changes in the quasiparticle density with temperature can be directly related to changes in the resonant frequency and dissipation using the Mattis-Bardeen equations by introducing β ; the ratio of the frequency response to the dissipation response. β is a function of the probe frequency f and temperature T and for a thermal quasiparticle distribution, it is given by the equation⁵²

$$\beta(f, T) = \frac{1 + \sqrt{\frac{2\Delta}{\pi k_B T}} \exp \left[-\frac{hf}{2k_B T} \right] I_0 \left[\frac{hf}{2k_B T} \right]}{\frac{2}{\pi} \sqrt{\frac{2\Delta}{\pi k_B T}} \sinh \left[\frac{hf}{2k_B T} \right] K_0 \left[\frac{hf}{2k_B T} \right]}. \quad (8)$$

K_0 and I_0 are the zeroth-order modified Bessel functions of the first and second order respectively. At our targeted $T_o = 380\text{mK}$ and $f \sim 300\text{MHz}$, $\beta \gg 1$. This means that the resonator frequency shift channel provides a larger signal for thermometry than the resonator dissipation. Using β , we find that $Q_i \delta_i = (\delta n_{\text{qp}}/n_{\text{qp}})$ and $Q_i \delta x = \frac{1}{2} \beta(f, T) (\delta n_{\text{qp}}/n_{\text{qp}})$.

We are now in a position to combine the thermal and electrical responses to obtain the power-to-frequency responsivity S of a TKID bolometer:

$$S \equiv \frac{\delta f_r}{\delta P_{\text{opt}}} = \frac{\partial f_r}{\partial x} \frac{\partial x}{\partial n_{\text{qp}}} \frac{\partial n_{\text{qp}}}{\partial T} \frac{\partial T}{\partial P_{\text{opt}}} = f_r(T) \frac{\kappa(T) \beta(f, T)}{2 Q_i G(T) T} \quad (9)$$

where

$$\kappa(T) \equiv \frac{d \ln n_{\text{qp}}}{d \ln T} = \left(\frac{1}{2} + \frac{\Delta}{k_B T} \right).$$

C. Other Noise Terms

The three remaining noise terms are: generation-recombination (gr), TLS, and amplifier noise from the readout chain. All the noise terms add in quadrature: $\text{NEP}_{\text{total}}^2 = \text{NEP}_{\text{photon}}^2 + \text{NEP}_{\text{ph}}^2 + \text{NEP}_{\text{gr}}^2 + \text{NEP}_{\text{amp}}^2 + \text{NEP}_{\text{TLS}}^2$. We consider each of these terms in turn and describe the conditions under which each of them remains sub-dominant to the phonon noise level.

a. Generation-recombination (gr) noise

Generation-recombination noise is present in TKIDs because quasiparticle production and recombination are random processes that fluctuate over time. Even so, the dynamics of the averaged quasiparticle population are well understood using non-equilibrium statistical mechanics⁶⁵. TKIDs operate at large quasiparticle densities where the quasiparticle recombination rate Γ_{rec} is quadratic in the quasiparticle density,

$$\Gamma_{\text{rec}} = \frac{1}{2} V_{\text{sc}} R n_{\text{qp}}^2, \quad (10)$$

where R is the recombination constant of the superconductor with volume V_{sc} . For small perturbations in the quasiparticle density about its mean, quasiparticles have a characteristic lifetime $\tau_{\text{qp}} = 1/(R \cdot n_{\text{qp}})$. It is important to note that the energy relaxation time is half the quasiparticle lifetime⁴². Accounting for this, the fluctuations in the quasiparticle number can be described by the one-sided power spectrum $S_{\text{gr}}(\nu)$ given as⁶⁵

$$S_{\text{gr}}(\nu) = \frac{2\tau_{\text{qp}} n_{\text{qp}} V_{\text{sc}}}{1 + (\pi\nu\tau_{\text{qp}})^2}. \quad (11)$$

The generation-recombination NEP is the square root of the power spectrum divided by $V_{\text{sc}}^2 \cdot (\partial n_{\text{qp}} / \partial P_{\text{opt}})^2$,

$$\text{NEP}_{\text{gr}} = \frac{G(T)T}{n_{\text{qp}}(T) \kappa(T)} \cdot \sqrt{\frac{2}{RV_{\text{sc}}}}. \quad (12)$$

Equation 12 shows that at high temperatures, gr noise is suppressed because the quasiparticle density increases exponentially with temperature. In addition, the responsivity, given in equation 9, is independent of the superconductor volume. As a result, we are free to make the inductor volume large to further suppress the gr noise. This is an additional degree of flexibility for TKIDs, unlike many KID designs in which the inductor volume must be kept small to keep the optical responsivity high^{52,66}. The freedom to use a large inductor also allows us to use lower readout frequencies at a fixed capacitor size or alternatively, use smaller capacitors to achieve the same readout frequency.

b. Two-Level System noise

TLS noise in resonators is sourced by fluctuations in the permittivity of amorphous dielectric in the resonator⁶⁷. These fluctuations couple to the electric field of the resonator. Unlike the noise terms already considered, there is no microscopic theory of TLS noise. Instead, we apply the semi-empirical TLS noise model which is extensively covered in Gao's thesis⁶⁸. TLS effects in the resonator also modify the internal quality factor and also introduce an additional temperature-dependent frequency shift. These two effects are given by

$$Q_{\text{TLS}}^{-1} = F \delta_{\text{TLS}} = F \delta_0 \tanh\left(\frac{hf}{2k_B T}\right) \cdot \frac{1}{\sqrt{1 + P_g/P_c}}, \quad (13)$$

$$x_{\text{TLS}} = \frac{F \delta_0}{\pi} \left[\text{Re} \left[\Psi \left(\frac{1}{2} + \frac{hf}{2j\pi k_B T} \right) \right] - \ln \left(\frac{hf}{k_B T} \right) \right]. \quad (14)$$

Here, δ_{TLS} is the TLS contribution to the dielectric loss tangent, F is a filling factor that accounts for the fraction of the total electrical energy of the resonator that is stored in the TLS hosting material, δ_0 is the loss tangent constant and Ψ is the digamma function⁶⁹. At a probe tone power P_g and tone frequency f , TLS effects introduce a power dependence to the quality factor characterized by a critical power P_c . The fractional frequency shift is expected to be only weakly power dependent and positive with temperature increase. In the limit that $k_B T \ll hf$, the TLS loss drops off as $1/T$. Our target operating temperature is high enough to allow us to ignore the TLS effects on the resonator frequency and quality factor and only use the Mattis Bardeen relations.

The TLS noise power spectrum S_{TLS} in Hz^{-1} in the limit of strong electric fields is given as^{52,68}

$$S_{\text{TLS}} [\text{Hz}^{-1}] = \kappa_{\text{TLS}}(\nu, f, T) \frac{\int_{V_{\text{TLS}}} |\vec{E}(\vec{r})|^3 d^3 r}{4 \left[\int_V |\varepsilon(\vec{r}) \vec{E}(\vec{r})|^2 d^3 r \right]^2}, \quad (15)$$

where $\kappa_{\text{TLS}}(\nu, f, T)$ captures the dependence on temperature and readout frequency, $\vec{E}(\vec{r})$ is the electric field, $\varepsilon(\vec{r})$ is the dielectric constant, V_{TLS} is the volume of the TLS hosting media and V is the total volume. The electric field terms exhibit the measured $P_g^{-1/2}$ dependence on the readout power.

In order to compare TLS noise in devices with different geometry and operating conditions, it is more useful to use the microwave photon number N instead of the electric field. $N = E/(hf_r)$, where the E is the energy stored in the resonator. $E = \frac{1}{2} \cdot Q_i \cdot \chi_c \chi_g \cdot P_g / (2\pi f_r)$, from the definition of the internal quality factor. We must also account for the known saturation of the power dependence of TLS effects at low electric fields⁶⁹. We can include this saturation factor and make the temperature and readout frequency dependence of κ_{TLS} explicit by rewriting S_{TLS} as

$$S_{\text{TLS}} [\text{Hz}^{-1}] = \kappa_{\text{TLS},0} \left(\frac{\nu}{300\text{MHz}} \right)^{-\alpha} \left(\frac{T}{380\text{mK}} \right)^{-\beta} (1 + N/N_c)^{-\gamma} \quad (16)$$

where $\kappa_{\text{TLS},0}$ is a constant that sets the overall TLS noise level. The exponents typically have measured values⁵² $\alpha = 1/2, \beta = 1.5 - 2$ and $\gamma = 1/2$ although other values for the exponents α and β , have been suggested⁷⁰⁻⁷³. N_c captures TLS saturation at $N \ll N_c$ with the correct limit when $N \gg N_c$. We estimate $N_c \sim 7 \times 10^6$ from measured TLS critical powers of our devices, $P_c \sim -95$ dBm. A few simple scaling relations between measured δ_{TLS} and $\kappa_{\text{TLS},0}$, which are useful for predicting TLS behavior, have been reported in literature⁷¹⁻⁷³. We do not refer to these but we instead consider measured noise levels for similarly designed devices presented in Figure 14 of Zmuidzinas' review⁵² to estimate $\kappa_{\text{TLS},0} \sim 8 \times 10^{-23} \text{ Hz}^{-1}$. We specify $T = T_o$ and $f = 300\text{MHz}$, to obtain an upper limit of $S_{\text{TLS}}(1\text{Hz}, T_o, -90\text{dBm}) \sim 4 \times 10^{-19} \text{ Hz}^{-1}$.

We can obtain the TLS NEP by dividing the TLS power spectrum by the power-to-fractional-frequency-shift responsivity

$$\text{NEP}_{\text{TLS}}^2 = \frac{1}{(\partial x / \partial P_{\text{opt}})^2} S_{\text{TLS}}. \quad (17)$$

In order to satisfy $\text{NEP}_{\text{TLS}}^2 \ll \text{NEP}_{\text{ph}}^2$, the following condition must hold:

$$S_{\text{TLS}} \ll 4\chi k_B T_o^2 G(T_o) \left(\frac{\partial x}{\partial P_{\text{opt}}} \right)^2. \quad (18)$$

When we specify our design parameters, the condition reduces to $S_{\text{TLS}} \ll 2.7 \times 10^{-17} \text{ Hz}^{-1}$. The condition is satisfied because of the high responsivity $\partial x / \partial P_{\text{opt}} = 331 \text{ ppm/pW}^{-1}$ at T_o . The two orders of magnitude gap between the expected TLS noise level and the upper tolerable limit gives us confidence that TLS noise will have negligible impact on our devices during normal operation.

c. Amplifier Noise

The last noise contribution to consider is the additive noise of the amplifier. For an amplifier with noise temperature T_N and and at readout power P_g , the NEP contribution is given by⁵²

$$\text{NEP}_{\text{amp}} = \frac{1}{(\partial x / \partial P_{\text{opt}})} \cdot \frac{Q_c}{2 Q_r^2} \sqrt{\frac{k_B T_N}{P_g}}. \quad (19)$$

The amplifier noise contribution can be made small by using an amplifier with a low enough noise temperature or by biasing the resonators with a large readout power. Cryogenic low noise amplifiers with $T_N < 10$ K are readily available commercially. However, we deliberately limit the bias power to operate the resonators in the linear kinetic inductance regime.

An optimized TKID bolometer has detector noise contributions, NEP_{gr} , NEP_{TLS} and NEP_{amp} below the phonon noise. Figure 2 shows the noise model of an aluminum TKID as a

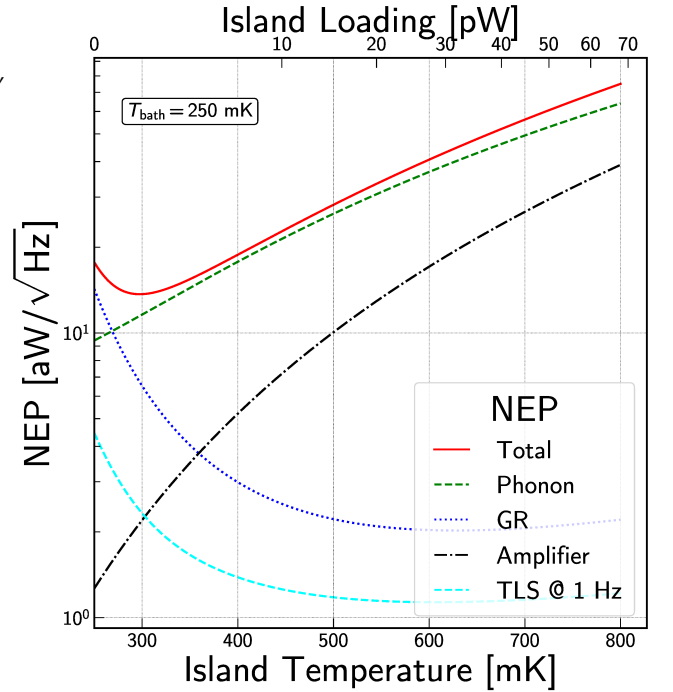


FIG. 2. Detector noise model of an aluminum TKID as a function of the island temperature showing each noise term. TLS noise was modeled using $\kappa_{\text{TLS},0} = 8 \times 10^{-23} \text{ Hz}^{-1}$ and the amplifier noise was calculated at a 5 K noise temperature and -90dBm readout power. The bolometer properties were chosen to match those of the 337 MHz resonator in table I and the resonator was taken to be optimally coupled at 380 mK.

function of the island temperature. The figure shows the limits under which generation-recombination vs. phonon noise dominates in the resonator. The bolometer parameters were chosen to be suitable for 150 GHz ground-based observations of the CMB. The resonator was taken to be optimally coupled at 380 mK and the readout power was set at -90 dBm with a 5 K amplifier noise temperature.

D. Device Design

We can apply the results from the previous subsections to determine an optimal design for TKID bolometers. First, since the phonon noise term dominates the internal noise, then the internal noise at the operating temperature is only a weak function of T_c . This means that a wide range of materials with T_c in the range 0.8 – 2 K can be used as background-limited detectors. We chose aluminum with $T_c \sim 1.2\text{K}$ as our superconductor for ease of fabrication. Using higher T_c materials could offer a multiplexing advantage because Q_r at the operating temperature increases with T_c .

We designed devices with relatively low resonance frequencies around 300 MHz. We designed each test chip with 5 TKIDs with a 15 MHz frequency spacing between resonators. The resonator circuits are built out of lithographed, lumped element inductors and capacitors. A fixed inductor geometry

was used for all the devices and each resonator has a unique main capacitor that sets the resonant frequency. Smaller coupling capacitors are used to set the coupling of the resonator to the readout line. Niobium with $T_c \sim 9$ K was used for all the capacitors and feedline structures so that the thermal response is solely attributable to the aluminum inductor. Figure 1 shows a simplified schematic of a TKID as well as a scanning electron microscope image of the bolometer island with the inductor and heater in view.

III. DETECTOR FABRICATION

We fabricated the detectors at the Microdevices Laboratory at the Jet Propulsion Laboratory (JPL) on 500 μm thick, high resistivity Si wafers⁵³. A low stress silicon nitride (LSN) layer, a niobium ground plane (GP) and a SiO_2 inter-layer dielectric (ILD) layer are deposited over the silicon. The LSN layer is then patterned to form the thermal island which is released using a XeF_2 etch process. The island is mechanically anchored to the main wafer via six LSN legs each about 10 μm wide. These legs make the weak thermal link from island to wafer. By selecting the length of the bolometer legs, we can also tune the thermal conductance. On each test chip, one device was fabricated with no island and the other 4 with bolometer leg lengths 100 μm , 200 μm , 300 μm and 400 μm . The island size was fixed to ~ 100 μm by ~ 500 μm for all the devices. This gives an expected heat capacity of 0.06 pJ/K, after accounting for both the dielectric (LSN and ILD) and metal (Nb and Al) layers⁷⁴⁻⁷⁶. The heat capacity is set by island volume of about 30,000 μm^3 , which is much larger than the combined volume of the bolometer legs of about 5,000 μm^3 for the longest leg bolometer. As a result, we expect that all the devices would have the same heat capacity. A small gold resistor added on the island is used for calibration and noise measurements(see Figure 1 (b)).

The aluminum layer of the inductor is deposited and patterned on the LSN. The meandered inductor traces are 50 nm thick and 1 μm wide with 1 μm spacing between the lines for a total volume of 810 μm^3 . Sonnet⁷⁷ simulations done assuming a surface inductance $L_s = 0.27$ pH/ \square , give a predicted geometric inductance, L_g of about 5 nH and a kinetic inductance fraction, $\alpha_k = 0.42$. The low film resistivity of aluminum limits the achievable kinetic inductance fraction.

The inter-digitated capacitors (IDC) are deposited directly on the crystalline Silicon wafer. The bare silicon is exposed by etching a large via through the ground plane (GP) and LSN layers. We did this to reduce the presence of amorphous dielectric that hosts two-level system⁶⁹ (TLS) effects from the capacitors. The via is large to minimize stray capacitive coupling between the ground plane and the edges of the capacitor, as determined by Sonnet simulations. An etch-back process was used to pattern the capacitors because liftoff often leaves flags that can potentially host TLS states.

IV. EXPERIMENTAL SETUP

We tested the devices in a Model 103 Rainier Adiabatic Demagnetization Refrigerator (ADR) cryostat from High Precision Devices (HPD)⁷⁸ with a Cryomech PT407 Pulse Tube Cryocooler⁷⁹. We used an external linear stepper drive motor to run the Pulse Tube in order to avoid RF pulses from a switching power supply. For mechanical stiffness, the ultra cold (UC) and intra cold (IC) stages of the cryostat are supported using long diameter Vespel tubes between the 4K stage and the IC and stiff titanium 15-3 alloy X-shaped crossbars between the IC and UC stages. Copper heat straps make the thermal contacts between the stages and the cold heads. The ADR reached a base temperature of 80 mK on the UC stage when the test chip was installed.

The RF connections between the UC and IC stages are through niobium-titanium (NbTi) coaxial cables with 10dB, 20dB and 30dB attenuators installed at the UC, IC and 4K stages respectively on the transmit side. At each thermal stage, the coaxial connections are heat sunk to the stage. A cold Low Noise Amplifier (LNA) is mounted at the 4K stage. The cold LNA is a SiGe HBT cryogenic amplifier from Caltech (CITLTF2)⁸⁰ with a measured noise temperature of 5.2 K with a 1.5 V bias. We also use a second amplifier with a noise temperature of 35 K at 5.0 V bias at room temperature.

For our data acquisition, we used the JPL-designed GPU accelerated system built on the Ettus Research USRP software defined radio (SDR) platform^{40,41}. 10 Gbit Ethernet connects the SDR to an Nvidia GPU, which handles the computationally heavy demodulation and analysis tasks in place of an FPGA. The SDR platform uses a 14 bit ADC and a 16 bit DAC and provides 120 MHz RF bandwidth.

The chip holder was sealed up with aluminum tape to make it light tight⁸¹. In addition, we anchored a Nb plate onto the UC stage to provide some shielding of the chip from the magnetic field of the ADR magnet.

V. RESULTS

For the device discussed here, we achieved a yield of 4/5 resonators. All the resonances were found in the frequency range 300-360 MHz and with close to the 15 MHz design spacing. The heaters of the 300, 200 and 100 μm leg bolometers were wired up to make calibrated noise and responsivity measurements.

A. Film Properties

Using four-point measurements of a test structure on chip, we measured $T_c = 1.284$ K, implying a superconducting gap energy, $\Delta = 1.95 \times 10^{-4}$ eV. The measured sheet resistance was $R_s = 0.25$ Ω/\square . R_s and Δ together give a surface inductance, $L_s = 0.27$ pH/ \square . Taking this value of L_s and accounting for the geometric inductance from simulations, gives an expected kinetic inductance fraction, $\alpha_k = 0.42$.

B. Resonator Properties and Modeling

We initially characterized the resonators using readout power sweeps at a fixed bath temperature of 80 mK and varying the power in the range, -110 dBm to -80 dBm. A key goal of this measurement was to determine the power level at the onset of the kinetic inductance non-linearity. In addition, changes in the quality factor with readout power probe two-level system effects.

We fit S_{21} using Swenson's nonlinear resonator model⁸². However, we found that our resonators could not be described adequately using the ideal S_{21} presented in equation 5. In general, parasitic inductance and capacitance, wirebond inductances, line mismatch and other effects modify the resonator line shape. In our experimental setup, these effects show up as an asymmetry in the resonator. An asymmetric line shape can be accounted for by making the coupling quality factor complex ($Q_c \rightarrow \hat{Q}_c$)^{62,63}; introducing an additional fitting parameter. Q_r and the real and imaginary parts of \hat{Q}_c are determined from the best fit to $S_{21}(f)$ and the internal quality factor Q_i is then recovered using $Q_i = (Q_r^{-1} - \Re[\hat{Q}_c^{-1}])^{-1}$. This relation motivates identifying 2 real quantities out of the complex \hat{Q}_c : the first being $Q_c = 1/\Re[\hat{Q}_c^{-1}]$ so that the equation $Q_r^{-1} = Q_i^{-1} + Q_c^{-1}$ holds; and the second, a coupling angle ϕ_c so that $\hat{Q}_c^{-1} = Q_c^{-1}(1 + j \tan \phi_c)$.

The coupling angle ϕ_c captures the resonator asymmetry since as $\phi_c \rightarrow 0$, $\hat{Q}_c \rightarrow Q_c$. Our resonators have a large ϕ_c in the range 0.4 – 0.7 radians. As tested by further simulations, we traced the asymmetry to about 7 pF of capacitive loading from short lengths of transmission line that branch from the readout line to the coupling capacitors.

Even up to -80 dBm we found that the bifurcation parameter defined by Swenson $a < 0.8$, implying that the resonators were always below the threshold for the bifurcation⁸². Informed by this, we chose a readout power of -90 dBm for all the other measurements that were done at a fixed readout power. At -90 dBm, the amplifier noise is sufficiently suppressed while keeping the readout power smaller than the heater loading on the TKID.

Q_i varies as a function of both the readout power P_g and the temperature T . We chose the following model to describe Q_i :

$$Q_i^{-1}(T, P_g) = Q_{\text{TLS}}^{-1}(T, P_g) + Q_{\text{MB}}^{-1}(T) + Q_{i,0}^{-1}, \quad (20)$$

where $Q_{\text{TLS}}^{-1}(T, P_g)$, is given in equation 13 and $Q_{\text{MB}}^{-1}(T)$ is the Mattis-Bardeen (MB) prediction⁵² and the third parameter $Q_{i,0}$ captures the saturation of Q_i at high power.

At 80 mK, the MB term is negligible and can be ignored for the power sweep measurements. Figure 3 shows Q_i as a function of the readout power for 4 yielded resonators. All four resonators have the product $F\delta_0 \approx 4.6 \times 10^{-5}$. Three of the resonators have $P_c \approx -95.7$ dBm and $Q_{i,0} \approx 4.4 \times 10^5$. The lower Q_i measured for the 305.9 MHz resonator implied a lower $Q_{i,0}$. Consistent with the TLS prediction, we found the fractional frequency shift with power to be negligibly small, peaking at about 5 ppm. Even so, TLS effects by themselves do not fully explain the power dependence because we found that $Q_{i,0}$ was needed in order to obtain good fits even though

it is not physically motivated. $Q_{i,0}$ may possibly come from a power dependence that is complicated by non-equilibrium quasiparticle distribution effects. This is still being actively investigated^{83,84}.

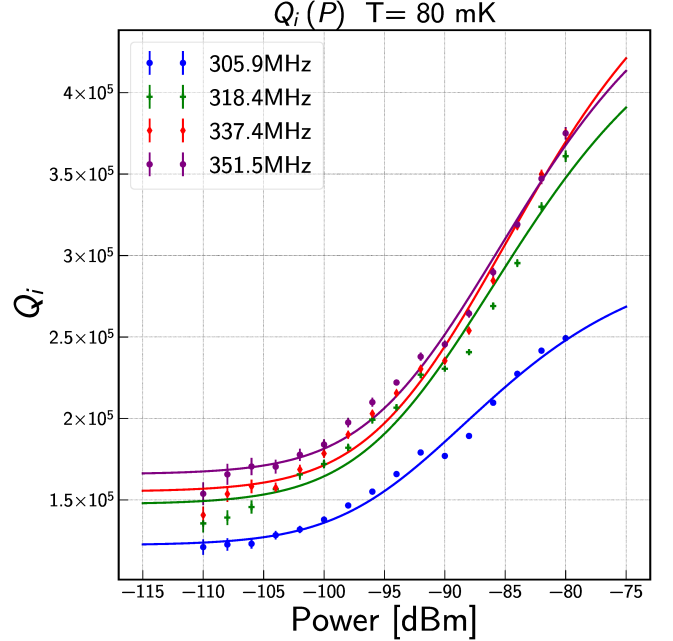


FIG. 3. Internal quality factor Q_i as a function of the readout power at 80 mK. The dots are the data and the solid lines are the fits to the data using the model described in equation 20.

S_{21} for each of the resonators was also measured as a function of the bath temperature. The readout power was fixed at -90 dBm and the temperature was swept up to 460 mK. This maximum temperature is high enough to break the degeneracy between the two MB parameters, α_k and T_c . At our operating temperature, these two parameters sufficiently describe our data as shown in figures 4 and 5 which summarize the fit results for the 337.4 MHz resonator.

At lower temperatures, however, the MB prediction fails because the quality factor levels off instead of increasing with a decrease in temperature. We compared three different models to describe this low temperature behavior: a pure MB prediction, a MB + TLS model and lastly, a model assuming a background quasiparticle population but no TLS. All three models were fit to only the frequency shift data and the best fit parameters were then used to make predictions of Q_i . The MB + TLS model best fit product $F\delta_0 \approx 3.4 \times 10^{-5}$ for all 4 resonators. However, this value of $F\delta_0$ gives a Q_{TLS}^{-1} that is too small for the data. In addition, if TLS effects were present, we would expect Q_i^{-1} to increase with decreasing temperature below about 200 mK. Such an increase is not consistent with the data.

A better fit was found using the background quasiparticle population n_{bg} model. In this case, total quasiparticle density is not simply the thermal quasiparticle density but rather it must be obtained by considering the balance of the quasiparticle generation and recombination rates⁶⁵. In addi-

tion, at low temperatures, empirical measurements show that quasiparticle lifetimes in Al resonators are described by the relation $\tau_{qp} = \tau_{max} / (1 + n_{qp}/n_{qp}^*)$. The two constants in the equation are n_{qp}^* , which is the crossover density and τ_{max} , which is the observed maximum lifetime^{52,85}. This new form of the quasiparticle lifetime has the expected inverse dependence on quasiparticle density in the limit of high n_{qp} . Because of this, we can relate the two new constants to the recombination constant as $R = 1 / (\tau_{max} n_{qp}^*)$. The quasiparticle density is now modified to

$$n_{qp}(T, n_{bg}) = \sqrt{(n_{th}(T) + n_{qp}^*)^2 + n_{bg}^2} - n_{qp}^* \quad (21)$$

Thermal and excess quasiparticles are equivalent in their effect on the electrodynamics of the superconductor⁸⁶. As a result, we can describe combined the effect of having both by defining an effective temperature T_{eff} using the relation $n_{qp}(T, n_{bg}) = n_{th}(T_{eff})$. The effective temperature was then used in place of T for all temperature dependent terms that determine the frequency shift and loss with n_{bg} as an additional parameter in the fitting. We have no measurements of n_{qp}^* for these devices, but we fixed its value based on later quasiparticle lifetime measurements done on similar TKIDs for which we found $n_{qp}^* = 518 \text{ um}^{-3}$ and $R = 5.3 \text{ um}^3 \text{ s}^{-1}$.

When comparing the best fit parameters from each of the three models, we found that the pure MB and the MB + TLS models give $T_c \approx 1.38\text{K}$ and $\alpha_k \approx 0.55$, which are much higher values than we obtained from the film measurements. The background quasiparticle model gave $T_c \approx 1.32\text{K}$ and $\alpha_k \approx 0.45$. On average over the 4 resonators, we found that $n_{bg} \approx 700 \text{ um}^{-3}$, corresponding to an effective temperature of about 150 mK. We estimate the recombination power, P_{recomb} from this population of quasiparticles as $P_{recomb} = \frac{1}{2} \cdot \Delta \cdot R \cdot n_{qp}^2 \cdot V_{sc} = 9 \text{ fW}$ which is about 1% of the readout power. The recombination power suggests that only a little additional loading on the bolometer is needed to account for the saturation of Q_i . A complete accounting of the low temperature quasiparticle dynamics in TKIDs as in many other KIDs has not been achieved. Even so, this does not affect TKID performance since our target operating temperature, $T_o = 380 \text{ mK}$ is well in the regime where our devices are fully characterized.

C. Thermal Conductivity and Bolometer Time Constants

By fixing the bath temperature and changing the power deposited by the heaters on the island, we can directly measure the thermal conductance and time constant.

The bath temperature, T_{bath} was fixed at 97 mK and S_{21} was measured at each heater bias power P . The island temperature T was then inferred from the resonance frequency shift using the best fit Mattis-Bardeen parameters α_k and Δ given in table I, assuming that $T = T_{bath}$ when the applied heater power is zero. The island temperature and bias power data are then fit to obtain the thermal conductivity coefficient K and power law index n .

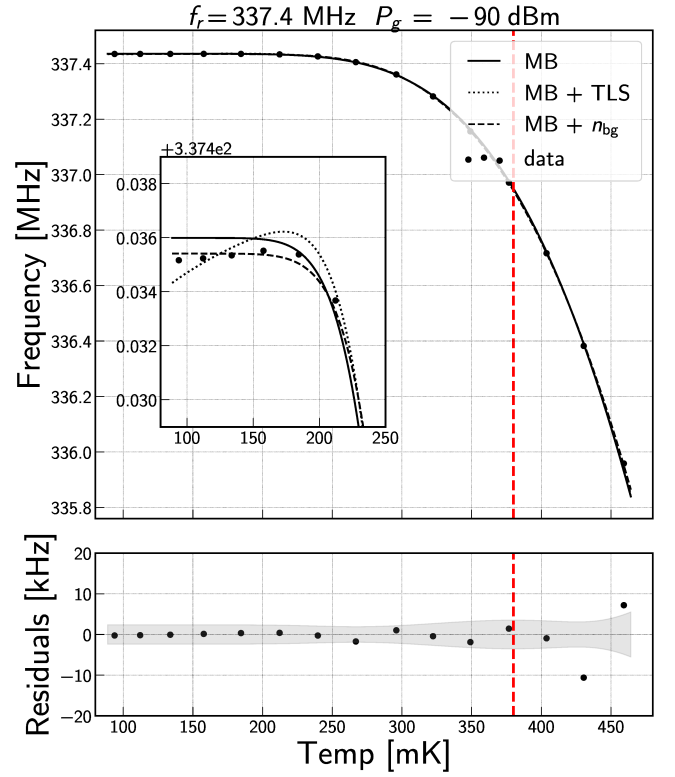


FIG. 4. Fits of the frequency shift data for the 337.4 MHz resonator to three different models: only MB, MB + TLS and MB + a background quasiparticle density. The inset plot has a much smaller x-axis range to better show the differences in the fits at low temperatures. The lower plot gives the fit residuals (black dots) and the one-sigma error obtained from the covariance of the fit parameters for the MB + background quasiparticle model (gray). The red dashed line is our target operating temperature of 380 mK.

Consistent with other similar bolometers used in BICEP/Keck⁵³, we measured $n \sim 3$. An index $n < 4$ indicates that phonon system has reduced dimensionality. We can motivate this physically, under the assumption that ballistic phonon propagation dominates over scattering in thermal transport. In this limit, the thermal phonon wavelength is given by $\lambda_{ph} = hc_s/k_B T$ where c_s is the speed of sound⁵³. We expect λ_{ph} to vary from 3.5 um at the 90 mK cold end to about 0.5 um at the 450 mK hot end for a speed of sound, $c_s \sim 6500 \text{ ms}^{-1}$ in silicon nitride. The nitride layer is only 0.3 um thick but the legs are 10 um wide and $300 - 500 \text{ um}$ long. Consequently, we expect thermal behavior consistent with a 2 dimensional phonon gas. The longitudinal sound velocity in silicon dioxide is comparable to that of silicon nitride so the same argument holds for thermal conduction through the similarly thick ILD layer. With the different bolometer leg lengths on the chip, we verified that the coefficient K , scales inversely with the bolometer leg length as shown in Table I. These observations are also supported by measurements of other silicon nitride bolometers that have reported similar values of n for bolometers with leg lengths $< 400 \text{ um}$ and width $> 2 \text{ um}$ ⁸⁷. As an additional step, we repeated

f_r [MHz]	Q_c	ϕ_c [rad]	T_c [K]	α_k	n_{bg} [μm^{-3}]	K [pW/K n]	n	C_0 [pJ/K $^{n+1}$]	η
305.9	15164 ± 72	0.6455 ± 0.0035	1.33 ± 0.01	0.46 ± 0.01	708 ± 10	352 ± 2	2.962 ± 0.009	1.943 ± 0.213	1.920 ± 0.115
318.4	17675 ± 104	0.7601 ± 0.0034	1.32 ± 0.09	0.45 ± 0.01	711 ± 10	165 ± 1	2.754 ± 0.012	1.839 ± 0.325	1.945 ± 0.184
337.4	22556 ± 129	0.7526 ± 0.0037	1.32 ± 0.01	0.45 ± 0.01	627 ± 9	122 ± 1	2.862 ± 0.011	1.742 ± 0.380	1.914 ± 0.219

TABLE I. Summary of the measured parameters of 3 TKID bolometers. The error bars on Q_c and ϕ_c were obtained from the spread in Q_e over power sweeps. α_k, T_c , were obtained from the bath temperature sweep data fit with a MB + background quasiparticle model. The K and n values reported here are from measurements done at a 250 mK bath temperature.

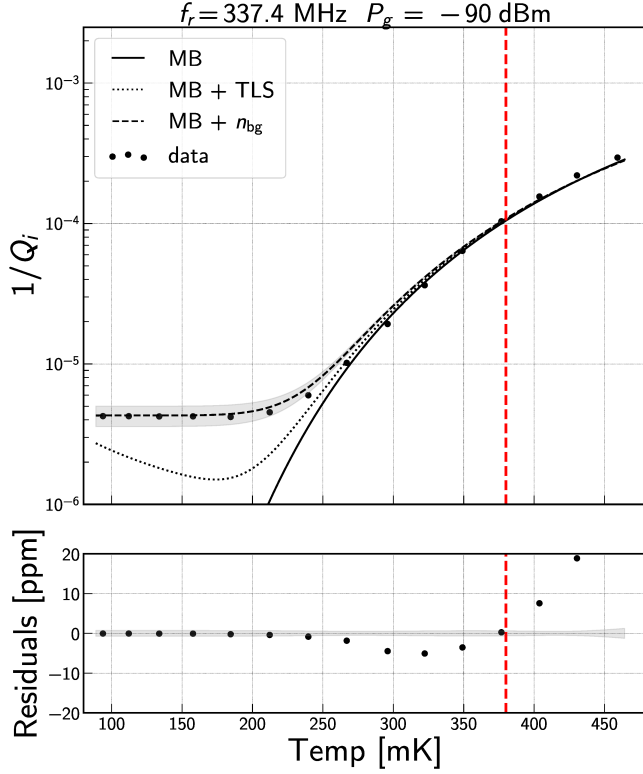


FIG. 5. A comparison of the measured Q_i to the best fit prediction for Q_i^{-1} obtained from fitting the frequency shift data as shown in figure 4. The best agreement between the data and the fit is with a MB + background quasiparticle density model. The lower plot gives the fit residuals (black dots) and the one-sigma error obtained from the covariance of the fit parameters for the MB + background quasiparticle model (gray). The red dashed line is our target operating temperature of 380 mK.

the thermal conductivity measurements at a second bath temperature, 249 mK as shown in figure 7. The extracted parameters were consistent with each other to about 10 %.

We define the optimal power P_{optimal} as the power needed to achieve the target island operating temperature, $T_o = 380$ mK. P_{optimal} is dependent on the bath temperature and is chosen so that the saturation power equals the expected loading seen during actual observations. At a 250 mK bath temperature, the 300 μm bolometer with a resonant frequency of 337.4 MHz has P_{optimal} appropriate for the expected loading at the South Pole at 150 GHz as shown in figures 6. The 100 μm and 200 μm designs are suitable for operating at 270 GHz and 220 GHz respectively under the same sky conditions.

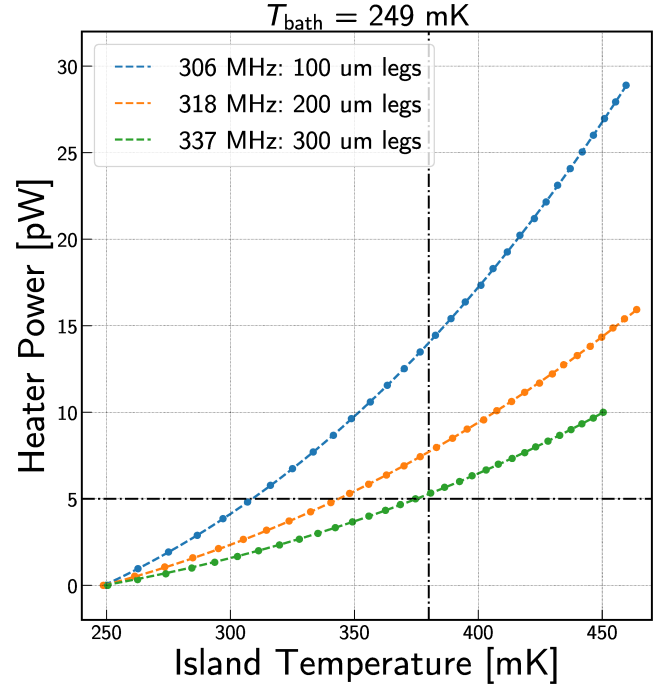


FIG. 6. Heater power plotted against the island temperature for 3 TKIDs showing agreement between the data (points) and best fit model (lines). The data was taken at a 250 mK bath temperature. The difference in slopes between the 3 curves is due to the difference in thermal conductivity of the three bolometers. The horizontal and vertical lines are the target loading and operating temperature respectively. These are well matched by the 300um leg bolometer.

We measured the bolometer time constants using a DC bias voltage plus an additional sine wave excitation was applied across the heater. The amplitude of the sine wave was about 1 % of the DC bias voltage. In addition, we synchronized the start of the data acquisition to the start of the sine wave excitation so that the phase of the input wave was always known. At each bias power, we stepped the excitation frequency of the input sine wave, f_{exc} , from 1 Hz to 1000 Hz in 30 logarithmically spaced steps.

We convert from the raw I/Q timestreams to resonance frequency and quality factor timestreams using the measured S_{21} parameters. By fitting the amplitude and phase of the change in resonance frequency with time, we obtained the complex bolometer transfer function, $H(f_{\text{exc}})$ which we model as a single-pole low-pass filter with rolloff frequency $f_{3dB} = 1/2\pi\tau_{\text{bolo}}$. The measured transfer function also includes the effect of the anti-aliasing filter used to decimate the data as

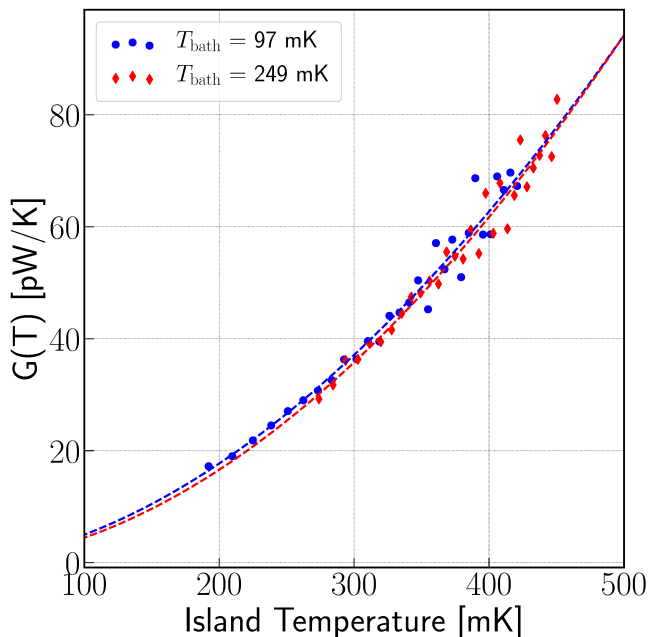


FIG. 7. The thermal conductance of the 337 MHz bolometer extracted at 2 bath temperatures. The data are given as the filled blue circles and red diamonds while the dotted lines are the best fit to a power law model. The fits show that the parameter K is independent of the bath temperature as expected.

well as unknown time delays in the trigger signal from the USRP to the function generator. Figure 8 shows the magnitude of the bolometer response with the single pole rolloff.

From these measurements, we conclude that the time constant for the 337 MHz TKID, $\tau \sim 4.5$ ms is fast enough for ground-based degree scale CMB observations. Interestingly, the time constants are weakly dependent on the island temperature. We expect the heat capacity to follow a simple power law $C = C_0 T^\eta$ and given that $\tau = C/G$, then this implies that $C \sim T^2$ as summarized in table I. Figure 9 confirms that the bulk of the heat capacity is from the island itself and not the bolometer legs. Additionally, the thermal island is almost entirely dielectric so we expect $\eta = 3$. The measured heat capacity is about a factor of 3 larger than predicted (see section III). Even without electro-thermal feedback, TKIDs are still fast enough for our targeted science band. There are indications that our dry release process using XeF_2 contributes to the excess heat capacity and that using a wet release process could lead to faster bolometers for space-based applications⁸⁸.

D. Responsivity

Over large ranges of the optical power, the responsivity of a TKID bolometer as given in equation 9 is not constant. However, during normal CMB observations, the optical power is typically stable to a few percent. In this case, the responsivity can be approximated as being constant with a small non-linearity correction. The non-linearity level is similar to

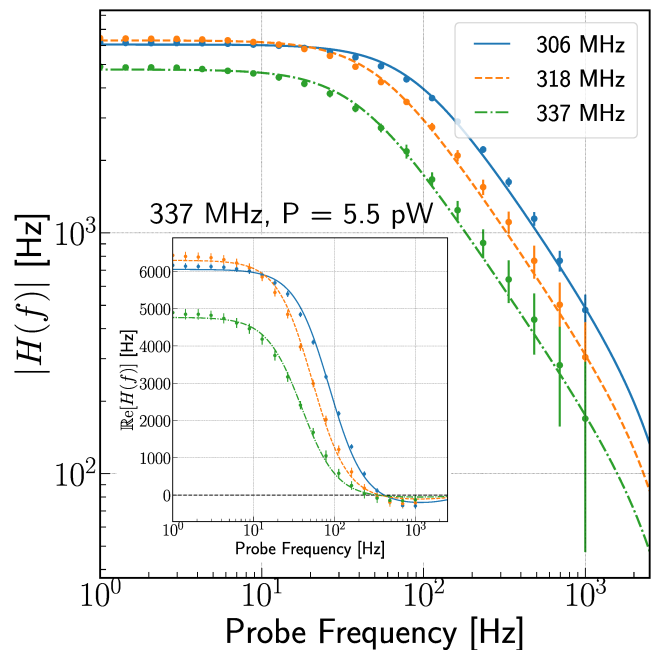


FIG. 8. A comparison between the magnitude and the real part of the bolometer transfer function measured at an 85 mK bath temperature and heater power of 5.5 pW for the 337 MHz bolometer. The data points have error bars enlarged by a factor of 10. The solid lines show the best fit to the model in equation 9. Inset is the real part of the bolometer response showing that response is modulated by the data filtering and additional time delays.

that of semiconducting NTD Ge bolometers that operate with small correction factors^{89,90}.

E. Noise Performance

The noise measurements were made by recording 10 minute long timestreams of the complex transmission at a 100 MHz native sample rate and then flat-averaging in 1000 sample blocks to a 100 kHz rate. A low noise, highly stable, Lakeshore 121 current source was used to DC bias the heater resistors. The power spectra of the resonance frequency timestream were estimated using the Welch method with a Hann window and a 50% overlap. In order to convert from power spectra in frequency units to NEP, we directly measured the responsivity in short calibration noise acquisitions by modulating the DC bias with a 1% 1 Hz square wave for 10 seconds. The responsivity is then estimated as the ratio of the change in frequency to the change in power dissipated.

The data were taken at a 80 mK bath temperature because the UC stage was less stable at 250 mK. At the same island temperature, the phonon noise with a 250 mK bath temperature is 30% higher than with a 80 mK bath. The measurement results presented here are focused on the 337 MHz resonator.

To simulate pair differencing, which is usually done when making on-sky polarization measurements, we subtracted out all the noise in the 337 MHz resonator that was common-

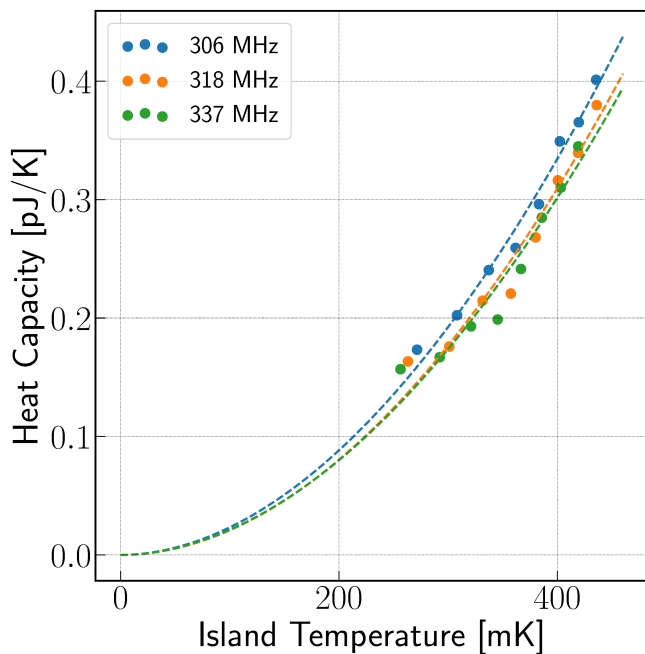


FIG. 9. Heat capacity for 3 TKID bolometers as a function of the island temperature. All three bolometers have similar heat capacities despite having different leg lengths showing that the island volume is the dominant contribution to the total heat capacity of the bolometer. The dashed lines are power law fits to the heat capacity as a function of the island temperature. The best fit parameters from each bolometer are consistent with each other to within a 1 sigma uncertainty as reported in table I.

mode with the other resonators as shown in figure 10. The origin of the common-mode signal is still under investigation but is likely from either the thermal fluctuations of the stage or RFI susceptibility. From the filtered timestream we computed the NEP at a 4 pW heater bias level. Given the lower bath temperature, the island temperature is 320 mK.

In the 4 pW noise dataset, the expected roll-off in the thermal responsivity at around 35 Hz is not visible. This indicates that at this loading, the device is in the regime where the gr noise dominates, giving the single roll-off seen at around 1 kHz as shown in figure 11. This figure also shows the comparison of the measured NEP to the noise model described in section II. However, our noise modeling is limited by our knowledge of the quasiparticle recombination constant R , which has not been directly measured for these devices. We instead modelled the noise by setting $R = 0.9 \mu\text{m}^3\text{s}^{-1}$ in order to match the gr noise roll-off seen at 4 pW loading with good agreement between the total noise from the model and the measured NEP.

A second set of noise data was taken at a 10 pW heater bias that corresponds to an island temperature of 422 mK; much higher than the operating temperature. Figure 12 shows a comparison of the measured noise at the two loading levels after common-mode subtraction. Even at the elevated island temperature, the measured NEP is still below the expected photon NEP. However, the NEP measured at the 10 pW level is about 2 times greater than expected from the noise model.

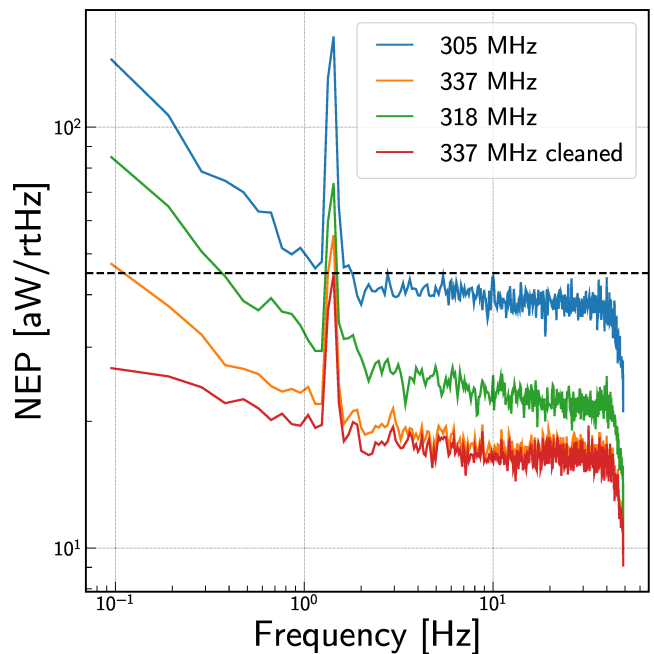


FIG. 10. NEP spectra for 3 TKID resonators with 4pW loading on the 337 MHz resonator. The red line shows the spectrum of the 337 MHz resonator with common mode noise subtraction applied to suppress the noise at low frequencies. The large spike is the 1.4 Hz pulse tube line. The black dotted line shows the expected photon noise level for a single-mode detector at the South Pole observing in a band centered at 150 GHz with $\Delta\nu/\nu = 0.25$.

This discrepancy is still under investigation. Also of note is that at the 10 pW loading level we see a roll-off in the noise where the thermal response is expected to fall off.

At both loading levels, total detector noise is lower than the expected photon NEP of $45 \text{ aW}/\sqrt{\text{Hz}}$ at the 4.7 pW loading for a ground-based CMB telescope observing in the 150 GHz band from the South Pole⁵⁹. We conclude that the device noise is low enough that a similar device coupled to an appropriate antenna^{91,92} would be background noise limited. Future work will focus on further understanding the gr noise and quasiparticle lifetimes in our devices.

VI. CONCLUSIONS

This paper presents a dark TKID design with detector noise that is low enough to produce background-limited performance when the device is appropriately coupled to an antenna tuned to observe in the 150 GHz frequency band from a ground-based CMB polarimeter. We've described the fundamental theory of TKID bolometer performance and compared it to actual devices. Our devices are fabricated using aluminum and niobium films deposited on a Silicon wafer using standard lithography techniques. We also presented the results from measurements of the film properties, bolometer characterization and dark noise measurements. Our device Q_i and f_r are well described using the Mattis-Bardeen theory at

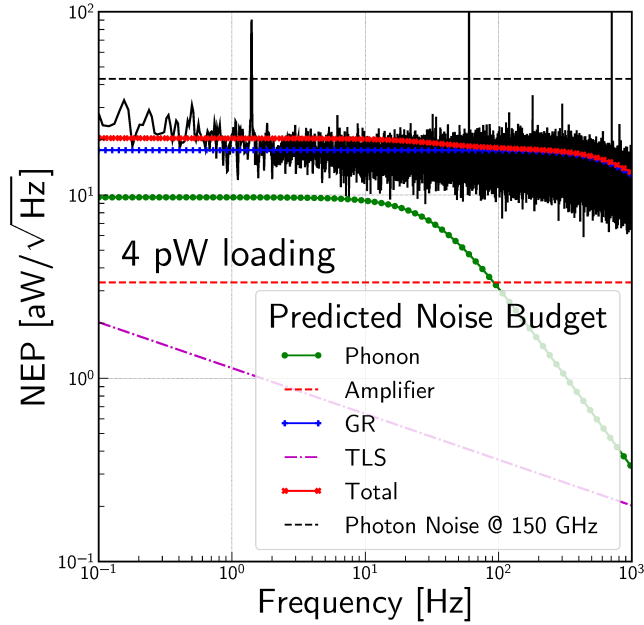


FIG. 11. NEP of the 337 MHz resonator with a 4pW loading. Overplotted are the estimated phonon, generation-recombination and amplifier noise contributions to the total noise based on the measured device parameters.

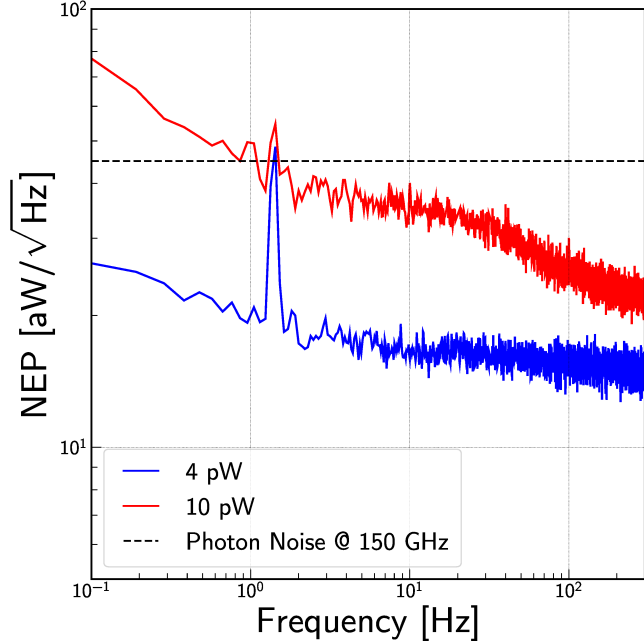


FIG. 12. A comparison of the measured NEP for the 337 MHz resonator at the 4 and 10 pW loading levels after common mode noise subtraction. The large spike at 1.4 Hz is the pulse tube line. At 10 pW, there is a clear roll-off in the noise at around 35 Hz. This is consistent with the predicted thermal noise roll-off from the thermal conductivity and heat capacity measurements. At 4 pW, this roll-off is not visible suggesting that the gr noise is dominant detector noise term since the island temperature is much lower.

our operating temperature.

Future work will focus on further understanding quasiparticle lifetimes in our devices, increasing the number of devices and better understanding the common mode environmental noise in our measurement system. We will also work to better understand the performance of our devices under high cosmic ray backgrounds. As reported by several groups, arrays of KIDs can be susceptible to cosmic ray events^{93,94}. Cosmic rays passing through a wafer generate ballistic phonons that propagate across the wafer, affecting multiple detectors. Cosmic rays thus cause extended dead-times because a single event affects multiple devices and because one must wait across several time constants for the response to decay. Cosmic ray susceptibility becomes even more important in space applications where event rates are significantly higher⁹⁵⁻⁹⁷. In TKIDs, the sensitive inductor is located on an island that is isolated from the entire wafer. The effective cross-section for interactions with cosmic rays is limited to the island instead of the entire wafer, greatly reducing our cosmic ray susceptibility. Other teams have reported similar results⁹³.

VII. ACKNOWLEDGEMENTS

The research was carried out at the Jet Propulsion Laboratory, California Institute of Technology, under contract with the National Aeronautics and Space Administration. We thank the JPL Research and Technology Development (RTD) program for supporting funds, as well as the Dominic Orr Graduate Fellowship in Physics at Caltech for supporting Mr. Wandui's graduate research. We are grateful to Warren Holmes for his early guidance on shaping this project.

VIII. DATA AVAILABILITY

The data that support the findings of this study are available from the corresponding author upon reasonable request.

IX. REFERENCES

- ¹R. Agnese, A. J. Anderson, D. Balakishiyeva, R. Basu Thakur, D. A. Bauer, A. Borgland, D. Brandt, P. L. Brink, R. Bunker, B. Cabrera, D. O. Caldwell, D. G. Cerdano, H. Chagani, M. Cherry, J. Cooley, B. Cornell, C. H. Crewdson, P. Cushman, M. Daal, P. C. F. Di Stefano, E. Do Couto E Silva, T. Doughty, L. Esteban, S. Fallows, E. Figueroa-Feliciano, J. Fox, M. Fritts, G. L. Godfrey, S. R. Golwala, J. Hall, H. R. Harris, J. Hasi, S. A. Hertel, B. A. Hines, T. Hofer, D. Holmgren, L. Hsu, M. E. Huber, A. Jastram, O. Kamaev, B. Kara, M. H. Kelsey, S. A. Kenany, A. Kennedy, C. J. Kenney, M. Kiveni, K. Koch, B. Loer, E. Lopez Asamar, R. Mahapatra, V. Mandic, C. Martinez, K. A. McCarthy, N. Mirabolfathi, R. A. Mofatt, D. C. Moore, P. Nadeau, R. H. Nelson, L. Novak, K. Page, R. Partridge, M. Pepin, A. Phipps, K. Prasad, M. Pyle, H. Qiu, R. Radpour, W. Rau, P. Redl, A. Reisetter, R. W. Resch, Y. Ricci, T. Saab, B. Sadoulet, J. Sander, R. Schmitt, K. Schneck, R. W. Schnee, S. Scorza, D. Seitz, B. Serfass, B. Shank, D. Speller, A. Tomada, A. N. Villano, B. Welliver, D. H. Wright, S. Yellin, J. J. Yen, B. A. Young, and J. Zhang, "Demonstration of surface electron rejection with interleaved germanium detectors for dark matter searches," *Applied Physics Letters* **103**, 164105 (2013), <https://doi.org/10.1063/1.4826093>.

- ²E. Armengaud, Q. Arnaud, C. Augier, A. Benoît, A. Benoît, L. Bergé, T. Bergmann, J. Billard, J. Blümler, T. de Boissière, G. Bres, A. Broniatowski, V. Brudanin, P. Camus, A. Cazes, M. Chapellier, F. Charlieux, L. Dumoulin, K. Eitel, D. Filosofov, N. Foerster, N. Fourches, G. Garde, J. Gascon, G. Gerbier, A. Giuliani, M. Grollier, M. Gros, L. Hehn, S. Hervé, G. Heuermann, V. Humbert, M. D. Jésus, Y. Jin, S. Jokisch, A. Juillard, C. Kéfélian, M. Kleifges, V. Kozlov, H. Kraus, V. Kudryavtsev, H. Le-Sueur, J. Lin, M. Mancuso, S. Marnieros, A. Menchikov, X.-F. Navick, C. Nones, E. Olivieri, P. Pari, B. Paul, M.-C. Piro, D. Poda, E. Queguiner, M. Robinson, H. Rodenas, S. Rozov, V. Sanglard, B. Schmidt, S. Scorza, B. Siebenborn, D. Tcherniakhovski, L. Vagneron, M. Weber, E. Yakushev, and X. Zhang, “Constraints on low-mass WIMPs from the EDELWEISS-III dark matter search,” *Journal of Cosmology and Astroparticle Physics* **2016**, 019–019 (2016).
- ³A. Abdelhameed *et al.* (CRESSST), “First results from the CRESSST-III low-mass dark matter program,” *Phys. Rev. D* **100**, 102002 (2019), arXiv:1904.00498 [astro-ph.CO].
- ⁴G. Angloher, P. Carniti, L. Cassina, L. Gironi, C. Gotti, A. Gütlein, D. Hauff, M. Maino, S. S. Nagorny, L. Pagnanini, G. Pessina, F. Petricca, S. Pirro, F. Pröbst, F. Reindl, K. Schäffner, J. Schieck, and W. Seidel, “The cosinus project: perspectives of a nai scintillating calorimeter for dark matter search,” *The European Physical Journal C* **76**, 441 (2016).
- ⁵K. Alfonso, D. R. Artusa, F. T. Avignone, O. Azzolini, M. Balata, T. I. Banks, G. Bari, J. W. Beeman, F. Bellini, A. Bersani, M. Biassoni, C. Brofferio, C. Bucci, A. Caminata, L. Canonica, X. G. Cao, S. D. Capelli, L. Cappelli, L. Carbone, L. Cardani, N. Casali, L. Cassina, D. Chiesa, N. Chott, M. Clemenza, S. Copello, C. Cosmelli, O. Cremonesi, R. J. Creswick, J. S. Cushman, I. Dafinei, A. Dally, S. Dell’Oro, M. M. Deninno, S. Di Domizio, M. L. Di Vacri, A. Drobizhev, L. Ejzack, D. Q. Fang, M. Faverezani, G. Fernandes, E. Ferri, F. Ferroni, E. Fiorini, S. J. Freedman, B. K. Fujikawa, A. Giachero, L. Gironi, A. Giuliani, P. Gorla, C. Gotti, T. D. Gutierrez, E. E. Haller, K. Han, E. Hansen, K. M. Heeger, R. Hennings-Yeomans, K. P. Hickerson, H. Z. Huang, R. Kadel, G. Keppel, Y. G. Kolomensky, K. E. Lim, X. Liu, Y. G. Ma, M. Maino, M. Martinez, R. H. Maruyama, Y. Mei, N. Moggi, S. Morganti, S. Nisi, C. Nones, E. B. Norman, A. Nucciotti, T. O’Donnell, F. Orto, D. Orlandi, J. L. Ouellet, C. E. Pagliarone, M. Pallavicini, V. Palmieri, L. Pattavina, M. Pavan, M. Pedretti, G. Pessina, V. Pettinacci, G. Piperno, S. Pirro, S. Pozzi, E. Previtali, C. Rosenfeld, C. Rusconi, E. Sala, S. Sangiorgio, D. Santone, N. D. Scielzo, M. Sisti, A. R. Smith, L. Taffarello, M. Tenconi, F. Terranova, C. Tomei, S. Trentalange, G. Ventura, M. Vignati, S. L. Wagaarachchi, B. S. Wang, H. W. Wang, L. Wielgus, J. Wilson, L. A. Winslow, T. Wise, L. Zantotti, C. Zarra, G. Q. Zhang, B. X. Zhu, and S. Zucchelli (CUORE Collaboration), “Search for neutrinoless double-beta decay of ^{130}Te with cuore-0,” *Phys. Rev. Lett.* **115**, 102502 (2015).
- ⁶Alpert, B., Balata, M., Bennett, D., Biasotti, M., Boragno, C., Brofferio, C., Ceriale, V., Corsini, D., Day, P. K., De Gerone, M., Dressler, R., Faverezani, M., Ferri, E., Fowler, J., Gatti, F., Giachero, A., Hays-Wehle, J., Heinitz, S., Hilton, G., Köster, U., Lusignoli, M., Maino, M., Mates, J., Nisi, S., Nizzolo, R., Nucciotti, A., Pessina, G., Pizzigoni, G., Puiu, A., Ragazzi, S., Reintsema, C., Gomes, M. Ribeiro, Schmidt, D., Schumann, D., Sisti, M., Swetz, D., Terranova, F., and Ullom, J., “Holmes - the electron capture decay of 163-ho to measure the electron neutrino mass with sub-eV sensitivity,” *Eur. Phys. J. C* **75**, 112 (2015).
- ⁷C. Hassel, K. Blaum, T. D. Goodacre, H. Dorrer, K. Eberhardt, S. Eliseev, C. Enss, P. Filianin, A. Fleischmann, L. Gastaldo, M. Goncharov, D. Hengstler, J. Jochum, K. Johnston, M. Keller, S. Kempf, T. Kieck, M. Krantz, B. Marsh, C. Mokry, Y. N. Novikov, P. C. O. Ranitzsch, S. Rothe, A. Rischka, J. Runke, A. Saenz, F. Schneider, S. Scholl, F. Simkovic, T. Stora, M. Veinhard, M. Wegner, K. Wendt, and K. Zuber, “Recent results for the echo experiment,” *Journal of Low Temperature Physics* **184**, 910–921 (2016).
- ⁸A. Luukanen, M. M. Leivo, A. Rautiainen, M. Grönholm, H. Toivanen, L. Grönberg, P. Helistö, A. Mäyrä, M. Aikio, E. N. Grossman, and A. Luukanen, “Applications of superconducting bolometers in security imaging,” *Journal of Physics: Conference Series* **400**, 052018 (2012).
- ⁹T. May, E. Heinz, K. Peiselt, G. Zieger, D. Born, V. Zakosarenko, A. Brömel, S. Anders, and H. G. Meyer, “Next generation of a sub-millimetre wave security camera utilising superconducting detectors,” *Journal of Instrumentation* **8**, P01014–P01014 (2013).
- ¹⁰H. Hui, P. A. R. Ade, Z. Ahmed, K. D. Alexander, M. Amiri, D. Barkats, S. J. Benton, C. A. Bischoff, J. J. Bock, H. Boenish, R. Bowens-Rubin, I. Buder, E. Bullock, V. Buza, J. Connors, J. P. Filippini, S. Fliescher, J. A. Grayson, M. Halpern, S. Harrison, G. C. Hilton, V. V. Hristov, K. D. Irwin, J. Kang, K. S. Karkare, E. Karpel, S. Kefeli, S. A. Kernasovskiy, J. M. Kovac, C. L. Kuo, E. M. Leitch, M. Lueker, K. G. Megerian, V. Monticue, T. Namikawa, C. B. Netterfield, H. T. Nguyen, R. O’Brien, R. W. O. IV, C. Pryke, C. D. Reintsema, S. Richter, R. Schwarz, C. Sorensen, C. D. Sheehy, Z. K. Staniszewski, B. Steinbach, G. P. Teply, K. L. Thompson, J. E. Tolan, C. Tucker, A. D. Turner, A. G. Viereg, A. Wandui, A. C. Weber, D. V. Wiebe, J. Willmert, W. L. K. Wu, and K. W. Yoon, “Bicep3 focal plane design and detector performance,” (2016).
- ¹¹B. A. Benson, P. A. R. Ade, Z. Ahmed, S. W. Allen, K. Arnold, J. E. Austermann, A. N. Bender, L. E. Bleem, J. E. Carlstrom, C. L. Chang, H. M. Cho, J. F. Cliche, T. M. Crawford, A. Cukierman, T. de Haan, M. A. Dobbs, D. Dutcher, W. Everett, A. Gilbert, N. W. Halverson, D. Hanson, N. L. Harrington, K. Hattori, J. W. Henning, G. C. Hilton, G. P. Holder, W. L. Holzapfel, K. D. Irwin, R. Keisler, L. Knox, D. Kubik, C. L. Kuo, A. T. Lee, E. M. Leitch, D. Li, M. McDonald, S. S. Meyer, J. Montgomery, M. Myers, T. Natoli, H. Nguyen, V. Novosad, S. Padin, Z. Pan, J. Pearson, C. Reichardt, J. E. Ruhl, B. R. Saliwanchik, G. Simard, G. Smecher, J. T. Sayre, E. Shirokoff, A. A. Stark, K. Story, A. Suzuki, K. L. Thompson, C. Tucker, K. Vanderlinde, J. D. Vieira, A. Vikhlinin, G. Wang, V. Yefremenko, and K. W. Yoon, “Spt-3g: a next-generation cosmic microwave background polarization experiment on the south pole telescope,” (2014).
- ¹²Z. D. Kermish, P. Ade, A. Anthony, K. Arnold, D. Barron, D. Boettger, J. Borrill, S. Chapman, Y. Chinone, M. A. Dobbs, J. Errard, G. Fabbian, D. Flanagan, G. Fuller, A. Ghribi, W. Grainger, N. Halverson, M. Hasegawa, K. Hattori, M. Hazumi, W. L. Holzapfel, J. Howard, P. Hyland, A. Jaffe, B. Keating, T. Kisner, A. T. Lee, M. L. Jeune, E. Linder, M. Lungu, F. Matsuda, T. Matsumura, X. Meng, N. J. Miller, H. Morii, S. Moyerman, M. J. Myers, H. Nishino, H. Paar, E. Quealy, C. L. Reichardt, P. L. Richards, C. Ross, A. Shimizu, M. Shimon, C. Shimmin, M. Sholl, P. Siritanasak, H. Spieler, N. Stebor, B. Steinbach, R. Stompor, A. Suzuki, T. Tomaru, C. Tucker, and O. Zahn, “The polarbear experiment,” (2012).
- ¹³S. W. Henderson, R. Allison, J. Austermann, T. Baidon, N. Battaglia, J. A. Beall, D. Becker, F. De Bernardis, J. R. Bond, E. Calabrese, S. K. Choi, K. P. Coughlin, K. T. Crowley, R. Datta, M. J. Devlin, S. M. Duff, J. Dunkley, R. Dünner, A. van Engelen, P. A. Gallardo, E. Grace, M. Hasselfield, F. Hills, G. C. Hilton, A. D. Hincks, R. Hlozek, S. P. Ho, J. Hubmayr, K. Huffenberger, J. P. Hughes, K. D. Irwin, B. J. Koopman, A. B. Kosowsky, D. Li, J. McMahon, C. Munson, F. Nati, L. Newburgh, M. D. Niemack, P. Niraula, L. A. Page, C. G. Pappas, M. Salatino, A. Schillaci, B. L. Schmitt, N. Sehgal, B. D. Sherwin, J. L. Sievers, S. M. Simon, D. N. Spergel, S. T. Staggs, J. R. Stevens, R. Thornton, J. Van Lanen, E. M. Vavagiakis, J. T. Ward, and E. J. Wollack, “Advanced actpol cryogenic detector arrays and readout,” *Journal of Low Temperature Physics* **184**, 772–779 (2016).
- ¹⁴T. Essinger-Hileman, A. Ali, M. Amiri, J. W. Appel, D. Araujo, C. L. Bennett, F. Boone, M. Chan, H.-M. Cho, D. T. Chuss, F. Colazo, E. Crowe, K. Denis, R. Dünner, J. Eimer, D. Gothe, M. Halpern, K. Harrington, G. C. Hilton, G. F. Hinshaw, C. Huang, K. Irwin, G. Jones, J. Karakla, A. J. Kogut, D. Larson, M. Limon, L. Lowry, T. Marriage, N. Mehrle, A. D. Miller, N. Miller, S. H. Moseley, G. Novak, C. Reintsema, K. Rostem, T. Stevenson, D. Towner, K. U-Yen, E. Wagner, D. Watts, E. J. Wollack, Z. Xu, and L. Zeng, “CLASS: the cosmology large angular scale surveyor,” in *Millimeter, Submillimeter, and Far-Infrared Detectors and Instrumentation for Astronomy* Vol. 9153, edited by W. S. Holland and J. Zmuidzinas, International Society for Optics and Photonics (SPIE, 2014) pp. 491–513.
- ¹⁵J. Lazaar, P. A. R. Ade, D. Benford, C. L. Bennett, D. T. Chuss, J. L. Dotson, J. R. Eimer, D. J. Fixsen, M. Halpern, G. Hilton, J. Hinderks, G. F. Hinshaw, K. Irwin, C. Jhabvala, B. Johnson, A. Kogut, L. Lowe, J. J. McMahon, T. M. Miller, P. Mirel, S. H. Moseley, S. Rodriguez, E. Sharp, J. G. Staguhn, E. R. Switzer, C. E. Tucker, A. Weston, and E. J. Wollack, “The Primordial Inflation Polarization Explorer (PIPER),” in *Millimeter, Submillimeter, and Far-Infrared Detectors and Instrumentation for Astronomy* Vol. 9153, edited by W. S. Holland and J. Zmuidzinas, International Society for Optics and Photonics (SPIE, 2014) pp. 529–539.

- ¹⁶M. C. Runyan, P. A. R. Ade, M. Amiri, S. Benton, R. Bihary, J. J. Bock, J. R. Bond, J. A. Bonetti, S. A. Bryan, H. C. Chiang, C. R. Contaldi, B. P. Crill, O. Dore, D. O’Dea, M. Farhang, J. P. Filippini, L. Fissel, N. Gandilo, S. R. Golwala, J. E. Gudmundsson, M. Hasselfield, M. Halpern, G. Hilton, W. Holmes, V. V. Hristov, K. D. Irwin, W. C. Jones, C. L. Kuo, C. J. MacTavish, P. V. Mason, T. A. Morford, T. E. Montroy, C. B. Netterfield, A. S. Rahlin, C. D. Reintsema, J. E. Ruhl, M. A. Schenker, J. Shariff, J. D. Soler, A. Trangsrud, R. S. Tucker, C. E. Tucker, and A. Turner, “Design and performance of the SPIDER instrument,” in *Millimeter, Submillimeter, and Far-Infrared Detectors and Instrumentation for Astronomy V*, edited by W. S. Holland and J. Zmuidzinas, International Society for Optics and Photonics (SPIE, 2010) pp. 497–508.
- ¹⁷B. Reichborn-Kjennerud, A. M. Aboobaker, P. Ade, F. Aubin, C. Baccigalupi, C. Bao, J. Borrill, C. Cantalupo, D. Chapman, J. Didier, M. Dobbs, J. Grain, W. Grainger, S. Hanany, S. Hillbrand, J. Hubmayr, A. Jaffe, B. Johnebson, T. Jones, T. Kisner, J. Klein, A. Korotkov, S. Leach, A. Lee, L. Levinson, M. Limon, K. MacDermid, T. Matsumura, X. Meng, A. Miller, M. Milligan, E. Pascale, D. Polsgrove, N. Ponthieu, K. Raach, I. Sagiv, G. Smecher, F. Stivoli, R. Stompfor, H. Tran, M. Tristram, G. S. Tucker, Y. Vinokurov, A. Yadav, M. Zaldarriaga, and K. Zilic, “EBEX: a balloon-borne CMB polarization experiment,” in *Millimeter, Submillimeter, and Far-Infrared Detectors and Instrumentation for Astronomy V*, edited by W. S. Holland and J. Zmuidzinas, International Society for Optics and Photonics (SPIE, 2010) pp. 381–392.
- ¹⁸J. Zhong, W. Zhang, W. Miao, D. Liu, Z. Wang, W. Duan, F. Wu, K. Zhang, Q. Yao, S. Shi, M. Wang, and F. Pajot, “Fast-response superconducting titanium bolometric detectors,” *IEEE Transactions on Applied Superconductivity* **29**, 1–5 (2019).
- ¹⁹J. N. Ullom and D. A. Bennett, “Review of superconducting transition-edge sensors for x-ray and gamma-ray spectroscopy,” *Superconductor Science and Technology* **28**, 084003 (2015).
- ²⁰K. D. Irwin and G. C. Hilton, “Transition-edge sensors,” in *Cryogenic Particle Detection*, edited by C. E. Ascheron, H. J. Koelsch, and W. Skolaut (Springer, Berlin, Heidelberg, Heidelberg, 2005) Chap. 3, pp. 63–150.
- ²¹*The SQUID Handbook* (John Wiley & Sons, Ltd, 2005) <https://onlinelibrary.wiley.com/doi/pdf/10.1002/3527603646.fmatter>.
- ²²P. A. J. de Korte, J. Beyer, S. Deiker, G. C. Hilton, K. D. Irwin, M. MacIntosh, S. W. Nam, C. D. Reintsema, L. R. Vale, and M. E. Huber, “Time-division superconducting quantum interference device multiplexer for transition-edge sensors,” *Review of Scientific Instruments* **74**, 3807–3815 (2003), <https://doi.org/10.1063/1.1593809>.
- ²³K. D. Irwin, L. R. Vale, N. E. Bergren, S. Deiker, E. N. Grossman, G. C. Hilton, S. W. Nam, C. D. Reintsema, D. A. Rudman, and M. E. Huber, “Time-division squid multiplexers,” *AIP Conference Proceedings* **605**, 301–304 (2002), <https://aip.scitation.org/doi/pdf/10.1063/1.1457650>.
- ²⁴M. A. Dobbs, M. Lueker, K. A. Aird, A. N. Bender, B. A. Benson, L. E. Bleem, J. E. Carlstrom, C. L. Chang, H.-M. Cho, J. Clarke, T. M. Crawford, A. T. Crites, D. I. Flanagan, T. de Haan, E. M. George, N. W. Halverson, W. L. Holzapfel, J. D. Hrubes, B. R. Johnson, J. Joseph, R. Keisler, J. Kennedy, Z. Kermish, T. M. Lanting, A. T. Lee, E. M. Leitch, D. Luong-Van, J. J. McMahon, J. Mehl, S. S. Meyer, T. E. Montroy, S. Padin, T. Plagge, C. Pryke, P. L. Richards, J. E. Ruhl, K. K. Schaffer, D. Schwan, E. Shirokoff, H. G. Spieler, Z. Staniszewski, A. A. Stark, K. Vanderlinde, J. D. Vieira, C. Vu, B. Westbrook, and R. Williamson, “Frequency multiplexed superconducting quantum interference device readout of large bolometer arrays for cosmic microwave background measurements,” *Review of Scientific Instruments* **83**, 073113 (2012), <https://doi.org/10.1063/1.4737629>.
- ²⁵M. Abitbol, A. M. Aboobaker, P. Ade, D. Araujo, F. Aubin, C. Baccigalupi, C. Bao, D. Chapman, J. Didier, M. Dobbs, S. M. Feeny, C. Geach, W. Grainger, S. Hanany, K. Helson, S. Hillbrand, G. Hilton, J. Hubmayr, K. Irwin, A. Jaffe, B. Johnson, T. Jones, J. Klein, A. Korotkov, A. Lee, L. Levinson, M. Limon, K. MacDermid, A. D. Miller, M. Milligan, K. Raach, B. Reichborn-Kjennerud, C. Reintsema, I. Sagiv, G. Smecher, G. S. Tucker, B. Westbrook, K. Young, and K. Zilic, “The EBEX balloon-borne experiment—detectors and readout,” *The Astrophysical Journal Supplement Series* **239**, 8 (2018).
- ²⁶H. Hui, P. A. R. Ade, Z. Ahmed, R. W. Aikin, K. D. Alexander, D. Barkats, S. J. Benton, C. A. Bischoff, J. J. Bock, R. Bowens-Rubin, J. A. Brevik, I. Buder, E. Bullock, V. Buza, J. Connors, J. Cornelson, B. P. Crill, M. Crumrine, M. Dierckx, L. Duband, C. Dvorkin, J. P. Filippini, S. Fliescher, J. Grayson, G. Hall, M. Halpern, S. Harrison, S. R. Hildebrandt, G. C. Hilton, K. D. Irwin, J. Kang, K. S. Karkare, E. Karpel, J. P. Kaufman, B. G. Keating, S. Kefeli, S. A. Kernasovskiy, J. M. Kovac, C.-L. Kuo, K. Lau, N. A. Larsen, E. M. Leitch, M. Lueker, K. G. Megerian, L. Moncelsi, T. Namikawa, C. B. Netterfield, H. T. Nguyen, R. O’Brien, R. W. O. IV, S. Palladino, C. Pryke, B. Racine, S. Richter, R. Schwarz, A. Schillaci, C. D. Sheehy, A. Soliman, T. S. Germaine, Z. K. Staniszewski, B. Steinbach, R. V. Sudiwala, G. P. Teply, K. L. Thompson, J. E. Tolan, C. Tucker, A. D. Turner, C. Umiltà, A. G. Vieregge, A. Wandui, A. C. Weber, D. V. Wiebe, J. Willmert, C. L. Wong, W. L. K. Wu, E. Yang, K. W. Yoon, and C. Zhang, “BICEP Array: a multi-frequency degree-scale CMB polarimeter,” in *Millimeter, Submillimeter, and Far-Infrared Detectors and Instrumentation for Astronomy V*, edited by J. Zmuidzinas and J.-R. Gao, International Society for Optics and Photonics (SPIE, 2018) pp. 1–15.
- ²⁷K. N. Abazajian, P. Adshead, Z. Ahmed, S. W. Allen, D. Alonso, K. S. Arnold, C. Baccigalupi, J. G. Bartlett, N. Battaglia, B. A. Benson, C. A. Bischoff, J. Borrill, V. Buza, E. Calabrese, R. Caldwell, J. E. Carlstrom, C. L. Chang, T. M. Crawford, F.-Y. Cyr-Racine, F. De Bernardis, T. de Haan, S. di Serego Alighieri, J. Dunkley, C. Dvorkin, J. Errard, G. Fabbian, S. Feeney, S. Ferraro, J. P. Filippini, R. Flauger, G. M. Fuller, V. Gluscevic, D. Green, D. Grin, E. Grohs, J. W. Henning, J. C. Hill, R. Hlozek, G. Holder, W. Holzapfel, W. Hu, K. M. Huffenberger, R. Keskitalo, L. Knox, A. Kosowsky, J. Kovac, E. D. Kovetz, C.-L. Kuo, A. Kusaka, M. Le Jeune, A. T. Lee, M. Lilley, M. Loverde, M. S. Madhavacheril, A. Mantz, D. J. E. Marsh, J. McMahon, P. D. Meerburg, J. Meyers, A. D. Miller, J. B. Munoz, H. N. Nguyen, M. D. Niemack, M. Peloso, J. Peloton, L. Pogosian, C. Pryke, M. Raveri, C. L. Reichardt, G. Rocha, A. Rotti, E. Schaaf, M. M. Schmittfull, D. Scott, N. Sehgal, S. Shandera, B. D. Sherwin, T. L. Smith, L. Sorbo, G. D. Starkman, K. T. Story, A. van Engelen, J. D. Vieira, S. Watson, N. Whitehorn, and W. L. Kimmy Wu, “CMB-S4 Science Book, First Edition,” arXiv e-prints, arXiv:1610.02743 (2016), arXiv:1610.02743 [astro-ph.CO].
- ²⁸P. K. Day, H. G. LeDuc, B. A. Mazin, A. Vayonakis, and J. Zmuidzinas, “A broadband superconducting detector suitable for use in large arrays,” *Nature* **425**, 817–821 (2003).
- ²⁹S. Doyle, P. Mauskopf, J. Naylon, A. Porch, and C. Duncombe, “Lumped element kinetic inductance detectors,” *Journal of Low Temperature Physics* **151**, 530–536 (2008).
- ³⁰B. A. Mazin, S. R. Meeker, M. J. Strader, P. Szypryt, D. Marsden, J. C. van Eyken, G. E. Duggan, A. B. Walter, G. Ulbricht, M. Johnson, B. Bumble, K. O’Brien, and C. Stoughton, “ARCONS: A 2024 pixel optical through near-IR cryogenic imaging spectrophotometer,” *Publications of the Astronomical Society of the Pacific* **125**, 1348–1361 (2013).
- ³¹C. M. McKenney, H. G. Leduc, L. J. Swenson, P. K. Day, B. H. Eom, and J. Zmuidzinas, “Design considerations for a background limited 350 micron pixel array using lumped element superconducting microresonators,” in *Millimeter, Submillimeter, and Far-Infrared Detectors and Instrumentation for Astronomy V*, edited by W. S. Holland, International Society for Optics and Photonics (SPIE, 2012) pp. 220–229.
- ³²A. Patel, A. Brown, W. Hsieh, T. Stevenson, S. H. Moseley, K. U-yen, N. Ehsan, E. Barrentine, G. Manos, and E. J. Wollack, “Fabrication of mkids for the microspec spectrometer,” *IEEE Transactions on Applied Superconductivity* **23**, 2400404–2400404 (2013).
- ³³S. R. Golwala, C. Bockstiegel, S. Brugger, N. G. Czakon, P. K. Day, T. P. Downes, R. Duan, J. Gao, A. K. Gill, J. Glenn, M. I. Hollister, H. G. LeDuc, P. R. Maloney, B. A. Mazin, S. G. McHugh, D. Miller, O. Noroozian, H. T. Nguyen, J. Sayers, J. A. Schlaertz, S. Siegel, A. K. Vayonakis, P. R. Wilson, and J. Zmuidzinas, “Status of MUSIC, the Multiwavelength Sub/millimeter Inductance Camera,” in *Millimeter, Submillimeter, and Far-Infrared Detectors and Instrumentation for Astronomy V*, edited by W. S. Holland, International Society for Optics and Photonics (SPIE, 2012) pp. 33–53.
- ³⁴A. Monfardini, A. Benoit, A. Bidaud, L. Swenson, A. Cruciani, P. Camus, C. Hoffmann, F. X. Désert, S. Doyle, P. Ade, P. Mauskopf, C. Tucker, M. Roesch, S. Leclercq, K. F. Schuster,

- A. Endo, A. Baryshev, J. J. A. Baselmans, L. Ferrari, S. J. C. Yates, O. Bourrion, J. Macias-Perez, C. Vescovi, M. Calvo, and C. Giordano, "A DUAL-BAND MILLIMETER-WAVE KINETIC INDUCTANCE CAMERA FOR THE IRAM 30 m TELESCOPE," *The Astrophysical Journal Supplement Series* **194**, 24 (2011).
- ³⁵B. J. Dober, P. A. R. Ade, P. Ashton, F. E. Angilè, J. A. Beall, D. Becker, K. J. Bradford, G. Che, H.-M. Cho, M. J. Devlin, L. M. Fissel, Y. Fukui, N. Galitzki, J. Gao, C. E. Groppi, S. Hillbrand, G. C. Hilton, J. Hubmayr, K. D. Irwin, J. Klein, J. V. Lanen, D. Li, Z.-Y. Li, N. P. Lourie, H. Mani, P. G. Martin, P. Mauskopf, F. Nakamura, G. Novak, D. P. Pappas, E. Pascale, F. P. Santos, G. Savini, D. Scott, S. Stanchfield, J. N. Ullom, M. Underhill, M. R. Vissers, and D. Ward-Thompson, "The next-generation BLASTPol experiment," in *Millimeter, Submillimeter, and Far-Infrared Detectors and Instrumentation for Astronomy VIII*, edited by W. S. Holland and J. Zmuidzinas, International Society for Optics and Photonics (SPIE, 2014) pp. 137 – 148.
- ³⁶A. Kovács, P. S. Barry, C. M. Bradford, G. Chattopadhyay, P. Day, S. Doyle, S. Hailey-Dunsheath, M. Hollister, C. McKenney, H. G. LeDuc, N. Llombart, D. P. Marrone, P. Mauskopf, R. C. O'Brien, S. Padin, L. J. Swenson, and J. Zmuidzinas, "SuperSpec: design concept and circuit simulations," in *Millimeter, Submillimeter, and Far-Infrared Detectors and Instrumentation for Astronomy VIII*, edited by W. S. Holland, International Society for Optics and Photonics (SPIE, 2012) pp. 748 – 757.
- ³⁷O. Bourrion, A. Benoit, J. Bouly, J. Bouvier, G. Bosson, M. Calvo, A. Catalano, J. Goupy, C. Li, J. Macías-Pérez, A. Monfardini, D. Tourres, N. Panchant, and C. Vescovi, "NIKEL-AMC: readout electronics for the NIKA2 experiment," *Journal of Instrumentation* **11**, P11001–P11001 (2016).
- ³⁸J. van Rantwijk, M. Grim, D. van Loon, S. Yates, A. Baryshev, and J. Baselmans, "Multiplexed readout for 1000-pixel arrays of microwave kinetic inductance detectors," *IEEE Transactions on Microwave Theory and Techniques* **64**, 1876–1883 (2016).
- ³⁹S. Gordon, B. Dober, A. Sinclair, S. Rowe, S. Bryan, P. Mauskopf, J. Austermann, M. Devlin, S. Dicker, J. Gao, G. C. Hilton, J. Hubmayr, G. Jones, J. Klein, N. P. Lourie, C. McKenney, F. Nati, J. D. Soler, M. Strader, and M. Vissers, "An open source, fpga-based lekid readout for blast-tng: Pre-flight results," *Journal of Astronomical Instrumentation* **05**, 1641003 (2016), <https://doi.org/10.1142/S2251171716410038>.
- ⁴⁰L. Minutolo, B. Steinbach, A. Wandui, and R. O'Brien, "A flexible gpu-accelerated radio-frequency readout for superconducting detectors," *IEEE Transactions on Applied Superconductivity* **29**, 1–5 (2019).
- ⁴¹L. Minutolo, "Gpu sdr," https://github.com/nasa/GPU_SDR (2019).
- ⁴²P. D. Mauskopf, "Transition edge sensors and kinetic inductance detectors in astronomical instruments," *Publications of the Astronomical Society of the Pacific* **130**, 082001 (2018).
- ⁴³J. E. Sauvageau and D. G. McDonald, "Superconducting kinetic inductance bolometer," *IEEE Transactions on Magnetics* **25**, 1331–1334 (1989).
- ⁴⁴G. Ulbricht, B. A. Mazin, P. Szypryt, A. B. Walter, C. Bockstiegel, and B. Bumble, "Highly multiplexible thermal kinetic inductance detectors for x-ray imaging spectroscopy," *Applied Physics Letters* **106**, 251103 (2015), <https://doi.org/10.1063/1.4923096>.
- ⁴⁵O. Quaranta, T. W. Cecil, L. Gades, B. Mazin, and A. Miceli, "X-ray photon detection using superconducting resonators in thermal quasi-equilibrium," *Superconductor Science and Technology* **26**, 105021 (2013).
- ⁴⁶M. Arndt, S. Wuensch, C. Groetsch, M. Merker, G. Zieger, K. Peiselt, S. Anders, H.-G. Meyer, and M. Siegel, "Optimization of the microwave properties of the kinetic-inductance bolometer (kibo)," *IEEE Transactions on Applied Superconductivity* **27**, 1–5 (2017).
- ⁴⁷A. V. Timofeev, V. Vesterinen, P. Heliöstö, L. Grönberg, J. Hassel, and A. Luukanen, "Submillimeter-wave kinetic inductance bolometers on free-standing nanomembranes," *Superconductor Science and Technology* **27**, 025002 (2013).
- ⁴⁸S. O. Dabironezare, J. Hassel, E. Gandini, L. Grönberg, H. Sipola, V. Vesterinen, and N. Llombart, "A dual-band focal plane array of kinetic inductance bolometers based on frequency-selective absorbers," *IEEE Transactions on Terahertz Science and Technology* **8**, 746–756 (2018).
- ⁴⁹R. A. Wernis, *Characterizing a resonator bolometer array*, Senior thesis, California Institute of Technology (2013).
- ⁵⁰D. Barron, Y. Chinone, A. Kusaka, J. Borril, J. Errard, S. Feeney, S. Ferraro, R. Keskitalo, A. T. Lee, N. A. Roe, B. D. Sherwin, and A. Suzuki, "Optimization study for the experimental configuration of CMB-s4," *Journal of Cosmology and Astroparticle Physics* **2018**, 009–009 (2018).
- ⁵¹B. A. Steinbach, J. J. Bock, H. T. Nguyen, R. C. O'Brien, and A. D. Turner, "Thermal kinetic inductance detectors for ground-based millimeter-wave cosmology," *Journal of Low Temperature Physics* **193**, 88–95 (2018).
- ⁵²J. Zmuidzinas, "Superconducting microresonators: Physics and applications," *Annual Review of Condensed Matter Physics* **3**, 169–214 (2012), <https://doi.org/10.1146/annurev-conmatphys-020911-125022>.
- ⁵³P. A. R. Ade, R. W. Aikin, M. Amiri, D. Barkats, S. J. Benton, C. A. Bischoff, J. J. Bock, J. A. Bonetti, J. A. Brevik, I. Buder, E. Bullock, G. Chattopadhyay, G. Davis, P. K. Day, C. D. Dowell, L. Duband, J. P. Filippini, S. Fliescher, S. R. Golwala, M. Halpern, M. Hasselfield, S. R. Hildebrandt, G. C. Hilton, V. Hristov, H. Hui, K. D. Irwin, W. C. Jones, K. S. Karkare, J. P. Kaufman, B. G. Keating, S. Kefeli, S. A. Kernasovskiy, J. M. Kovac, C. L. Kuo, H. G. LeDuc, E. M. Leitch, N. Llombart, M. Lueker, P. Mason, K. Megerian, L. Monceli, C. B. Netterfield, H. T. Nguyen, R. O'Brien, R. W. O. IV, A. Orlando, C. Pryke, A. S. Rahlin, C. D. Reintsema, S. Richter, M. C. Runyan, R. Schwarz, C. D. Sheehy, Z. K. Staniszewski, R. V. Sudiwala, G. P. Teply, J. E. Tolan, A. Trangsud, R. S. Tucker, A. D. Turner, A. G. Vieregg, A. Weber, D. V. Wilton, P. Wilson, C. L. Wong, K. W. Yoon, and J. Zmuidzinas, "Antenna-Coupled TES Bolometers used in BICEP2, Keck Array, and SPIDER," *The Astrophysical Journal* **812**, 176 (2015).
- ⁵⁴J. C. Mather, "Bolometer noise: Nonequilibrium theory," *Applied Optics* **21** (1982).
- ⁵⁵S. Pirro and P. Mauskopf, "Advances in bolometer technology for fundamental physics," *Annual Review of Nuclear and Particle Science* **67**, 161–181 (2017), <https://doi.org/10.1146/annurev-nucl-101916-123130>.
- ⁵⁶M. A. Lindeman, "Resonator-bolometer theory, microwave read out, and kinetic inductance bolometers," *Journal of Applied Physics* **116**, 024506 (2014).
- ⁵⁷J. C. Mather, "Bolometers: ultimate sensitivity, optimization, and amplifier coupling," *Applied Optics* **23** (1984).
- ⁵⁸P. L. Richards, "Bolometers for infrared and millimeter waves," *American Institute of Physics* **76** (1994), 10.1063/1.357128.
- ⁵⁹P. A. R. Ade, R. W. Aikin, M. Amiri, D. Barkats, S. J. Benton, C. A. Bischoff, J. J. Bock, J. A. Brevik, I. Buder, E. Bullock, G. Davis, P. K. Day, C. D. Dowell, L. Duband, J. P. Filippini, S. Fliescher, S. R. Golwala, M. Halpern, M. Hasselfield, S. R. Hildebrandt, G. C. Hilton, K. D. Irwin, K. S. Karkare, J. P. Kaufman, B. G. Keating, S. A. Kernasovskiy, J. M. Kovac, C. L. Kuo, E. M. Leitch, N. Llombart, M. Lueker, C. B. Netterfield, H. T. Nguyen, R. O'Brien, R. W. Ogburn, A. Orlando, C. Pryke, C. D. Reintsema, S. Richter, R. Schwarz, C. D. Sheehy, Z. K. Staniszewski, K. T. Story, R. V. Sudiwala, G. P. Teply, J. E. Tolan, A. D. Turner, A. G. Vieregg, P. Wilson, C. L. Wong, and K. W. Y. and, "BICEP2. II. EXPERIMENT AND THREE-YEAR DATA SET," *The Astrophysical Journal* **792**, 62 (2014).
- ⁶⁰E. A. Williams, S. Withington, C. N. Thomas, D. J. Goldie, and D. Osman, "Superconducting transition edge sensors with phononic thermal isolation," *Journal of Applied Physics* **124**, 144501 (2018), <https://doi.org/10.1063/1.5041348>.
- ⁶¹J. Zmuidzinas, "Thermal noise and correlations in photon detection," *Appl. Opt.* **42**, 4989–5008 (2003).
- ⁶²M. S. Khalil, M. J. A. Stoutimore, F. C. Wellstood, and K. D. Osborn, "An analysis method for asymmetric resonator transmission applied to superconducting devices," *Journal of Applied Physics* **111**, 054510 (2012), <https://doi.org/10.1063/1.3692073>.
- ⁶³C. Deng, M. Otto, and A. Lupascu, "An analysis method for transmission measurements of superconducting resonators with applications to quantum-regime dielectric-loss measurements," *Journal of Applied Physics* **114**, 054504 (2013), <https://doi.org/10.1063/1.4817512>.
- ⁶⁴M. Tinkham, *Introduction to superconductivity* Michael Tinkham (McGraw-Hill New York, 1996) pp. xix, 454 p. .
- ⁶⁵C. M. Wilson and D. E. Prober, "Quasiparticle number fluctuations in superconductors," *Phys. Rev. B* **69**, 094524 (2004).
- ⁶⁶H. McCarrick, D. Flanagan, G. Jones, B. R. Johnson, P. Ade, D. Araujo, K. Bradford, R. Cantor, G. Che, P. Day, S. Doyle, H. Leduc, M. Limon, V. Luu, P. Mauskopf, A. Miller, T. Mroczkowski,

- C. Tucker, and J. Zmuidzinas, "Horn-coupled, commercially-fabricated aluminum lumped-element kinetic inductance detectors for millimeter wavelengths," *Review of Scientific Instruments* **85**, 123117 (2014), <https://doi.org/10.1063/1.4903855>.
- ⁶⁷W. A. Phillips, "Two-level states in glasses," *Reports on Progress in Physics* **50**, 1657–1708 (1987).
- ⁶⁸J. Gao, *The Physics of Superconducting Microwave Resonators*, Ph.D. thesis, California Institute of Technology (2008).
- ⁶⁹J. Gao, M. Daal, A. Vayonakis, S. Kumar, J. Zmuidzinas, B. Sadoulet, B. A. Mazin, P. K. Day, and H. G. Leduc, "Experimental evidence for a surface distribution of two-level systems in superconducting lithographed microwave resonators," *Applied Physics Letters* **92**, 152505 (2008), <https://doi.org/10.1063/1.2906373>.
- ⁷⁰G. Frossati, J. leG Gilchrist, J. C. Lasjaunias, and W. Meyer, "Spectrum of low-energy dipolar states in hydrated vitreous silica," *Journal of Physics C: Solid State Physics* **10**, L515–L519 (1977).
- ⁷¹J. Burnett, L. Faoro, and T. Lindström, "Analysis of high quality superconducting resonators: consequences for TLS properties in amorphous oxides," *Superconductor Science and Technology* **29**, 044008 (2016).
- ⁷²A. N. Ramanayaka, B. Sarabi, and K. D. Osborn, "Evidence for universal relationship between the measured $1/f$ permittivity noise and loss tangent created by tunneling atoms," *arXiv e-prints*, arXiv:1507.06043 (2015), arXiv:1507.06043 [cond-mat.supr-con].
- ⁷³A. L. Burin, S. Matiyahu, and M. Schechter, "Low-temperature $1/f$ noise in microwave dielectric constant of amorphous dielectrics in josephson qubits," *Phys. Rev. B* **92**, 174201 (2015).
- ⁷⁴G. Wang, V. Yefremenko, V. Novosad, A. Datesman, J. Pearson, G. Shustakova, R. Divan, C. Chang, J. McMahon, L. Bleem, A. T. Crites, T. Downes, J. Mehl, S. S. Meyer, and J. E. Carlstrom, "Thermal properties of silicon nitride beams below 1 kelvin," *AIP Conference Proceedings* **1219**, 75–82 (2010), <https://aip.scitation.org/doi/pdf/10.1063/1.3402336>.
- ⁷⁵W. A. E. Phillips, *Amorphous Solids, Low-Temperature Properties* (Springer-Verlag Berlin Heidelberg, 1981) pp. xi, 179 p. .
- ⁷⁶R. Corruccini and J. Gniewek, *Specific Heats and Enthalpies of Technical Solids at Low Temperatures. A Compilation from the Literature*, NBS Monograph 21 (U.S. Government Printing Office, Washington, DC, 1960).
- ⁷⁷Sonnet Software, Inc., "High frequency electromagnetics software, sonnet release 13.0," [Online; accessed 13-January-2020].
- ⁷⁸High Precision Devices, Inc., "Cryostat model 103 rainier," [Online; accessed 13-January-2020].
- ⁷⁹Cryomech, "Pt407 cryocoolers," [Online; accessed 13-January-2020].
- ⁸⁰Cosmic Microwave Technology Inc., "Citf2 cryogenic low noise amplifier," [Online; accessed 13-January-2020].
- ⁸¹R. Barends, J. Wenner, M. Lenander, Y. Chen, R. C. Bialczak, J. Kelly, E. Lucero, P. O'Malley, M. Mariantoni, D. Sank, H. Wang, T. C. White, Y. Yin, J. Zhao, A. N. Cleland, J. M. Martinis, and J. J. A. Baselmans, "Minimizing quasiparticle generation from stray infrared light in superconducting quantum circuits," *Applied Physics Letters* **99**, 113507 (2011), <https://doi.org/10.1063/1.3638063>.
- ⁸²L. J. Swenson, P. K. Day, B. H. Eom, H. G. Leduc, N. Lombart, C. M. McKenney, O. Noroozian, and J. Zmuidzinas, "Operation of a titanium nitride superconducting microresonator detector in the nonlinear regime," *Journal of Applied Physics* **113**, 104501 (2013), <https://doi.org/10.1063/1.4794808>.
- ⁸³D. J. Goldie and S. Withington, "Non-equilibrium superconductivity in quantum-sensing superconducting resonators," *Superconductor Science and Technology* **26**, 015004 (2012).
- ⁸⁴P. de Visser, D. J. Goldie, P. Diener, S. Withington, J. J. A. Baselmans, and T. M. Klapwijk, "Evidence of a nonequilibrium distribution of quasiparticles in the microwave response of a superconducting aluminum resonator," *Phys. Rev. Lett.* **112**, 047004 (2014).
- ⁸⁵R. Barends, J. J. A. Baselmans, S. J. C. Yates, J. R. Gao, J. N. Hovenier, and T. M. Klapwijk, "Quasiparticle relaxation in optically excited high- q superconducting resonators," *Phys. Rev. Lett.* **100**, 257002 (2008).
- ⁸⁶J. Gao, J. Zmuidzinas, A. Vayonakis, P. Day, B. Mazin, and H. Leduc, "Equivalence of the Effects on the Complex Conductivity of Superconducting due to Temperature Change and External Pair Breaking," *Journal of Low Temperature Physics* **151**, 557–563 (2008).
- ⁸⁷S. Withington, E. Williams, D. J. Goldie, C. N. Thomas, and M. Schneiderman, "Thermal elastic-wave attenuation in low-dimensional sinter bars at low temperatures," *Journal of Applied Physics* **122**, 054504 (2017), <https://doi.org/10.1063/1.4997466>.
- ⁸⁸A. D. Beyer, M. E. Kenyon, P. M. Echternach, B.-H. Eom, J. Bueno, P. K. Day, J. J. Bock, and C. M. Bradford, "Characterizing SixNy absorbers and support beams for far-infrared/submillimeter transition-edge sensors," in *Millimeter, Submillimeter, and Far-Infrared Detectors and Instrumentation for Astronomy*, Vol. 7741, edited by W. S. Holland and J. Zmuidzinas, International Society for Optics and Photonics (SPIE, 2010) pp. 594 – 603.
- ⁸⁹Pajot, F., Ade, P. A. R., Beney, J.-L., Bréelle, E., Broszkiewicz, D., Camus, P., Carabétian, C., Catalano, A., Chardin, A., Charra, M., Charra, J., Cizeyron, R., Couchot, F., Coulais, A., Crill, B. P., Dassas, K., Daubin, J., de Bernardis, P., de Marcillac, P., Delouis, J.-M., Désert, F.-X., Duret, P., Eng, P., Evesque, C., Fourmond, J.-J., François, S., Giard, M., Giraud-Héraud, Y., Guglielmi, L., Guyot, G., Haissinski, J., Henrot-Versillé, S., Hervier, V., Holmes, W., Jones, W. C., Lamarre, J.-M., Lami, P., Lange, A. E., Lefebvre, M., Leriche, B., Leroy, C., Macias-Perez, J., Maciaszek, T., Maffei, B., Mahendran, A., Mansoux, B., Marty, C., Masi, S., Mercier, C., Miville-Deschênes, M.-A., Montier, L., Nicolas, C., Noviello, F., Perdereau, O., Piacentini, F., Piat, M., Plaszczyński, S., Pointecouteau, E., Pons, R., Ponthieu, N., Puget, J.-L., Rambaud, D., Renault, C., Renault, J.-C., Rioux, C., Ristorcelli, I., Rosset, C., Savini, G., Sudiwala, R., Torre, J.-P., Tristram, M., Vallée, D., Veneziani, M., and Yvon, D., "Planck pre-launch status: Hfi ground calibration," *A&A* **520**, A10 (2010).
- ⁹⁰Planck Collaboration, Adam, R., Ade, P. A. R., Aghanim, N., Arnaud, M., Ashdown, M., Aumont, J., Baccigalupi, C., Banday, A. J., Barreiro, R. B., Bartolo, N., Battaner, E., Benabed, K., Benoît, A., Benoit-Lévy, A., Bernard, J.-P., Bersanelli, M., Bertincourt, B., Bielewicz, P., Bock, J. J., Bonavera, L., Bond, J. R., Borrill, J., Bouchet, F. R., Boulanger, F., Bucher, M., Burigana, C., Calabrese, E., Cardoso, J.-F., Catalano, A., Challinor, A., Chamballu, A., Chary, R.-R., Chiang, H. C., Christensen, P. R., Clements, D. L., Colombi, S., Colombo, L. P. L., Combet, C., Couchot, F., Coulais, A., Crill, B. P., Curto, A., Cuttaia, F., Danese, L., Davies, R. D., Davis, R. J., de Bernardis, P., de Rosa, A., de Zotti, G., Delabrouille, J., Delouis, J.-M., Désert, F.-X., Diego, J. M., Dole, H., Donzelli, S., Doré, O., Douspis, M., Ducout, A., Dupac, X., Efstathiou, G., Elsner, F., Enßlin, T. A., Eriksen, H. K., Falgarone, E., Fergusson, J., Finelli, F., Forri, O., Frailis, M., Fraisse, A. A., Franceschi, E., Frejsel, A., Galeotta, S., Galli, S., Ganga, K., Ghosh, T., Giard, M., Giraud-Héraud, Y., Gjerløw, E., González-Nuevo, J., Górski, K. M., Gratton, S., Gruppuso, A., Gudmundsson, J. E., Hansen, F. K., Hanson, D., Harrison, D. L., Henrot-Versillé, S., Herranz, D., Hildebrandt, S., Hivon, E., Hobson, M., Holmes, W. A., Hornstrup, A., Hovest, W., Huffenberger, K. M., Hurier, G., Jaffe, A. H., Jaffe, T. R., Jones, W. C., Juvela, M., Keihänen, E., Keskitalo, R., Kisner, T. S., Kneissl, R., Knoch, J., Kunz, M., Kurki-Suonio, H., Lagache, G., Lamarre, J.-M., Lasenby, A., Lattanzi, M., Lawrence, C. R., Le Jeune, M., Leahy, J. P., Lellouch, E., Leonardi, R., Lesgourgues, J., Levrier, F., Liguori, M., Lilje, P. B., Linden-Vørnle, M., López-Cañiego, M., Lubin, P. M., Macías-Pérez, J. F., Maggio, G., Maino, D., Mandolesi, N., Mangilli, A., Maris, M., Martin, P. G., Martínez-González, E., Masi, S., Matarrese, S., McGehee, P., Melchiorri, A., Mendes, L., Mennella, A., Migliaccio, M., Mitra, S., Miville-Deschênes, M.-A., Moneti, A., Montier, L., Moreno, R., Morgante, G., Mortlock, D., Moss, A., Mottet, S., Munshi, D., Murphy, J. A., Naselsky, P., Nati, F., Natoli, P., Netterfield, C. B., Nørgaard-Nielsen, H. U., Noviello, F., Novikov, D., Novikov, I., Oxborrow, C. A., Paci, F., Pagano, L., Pajot, F., Paoletti, D., Pasian, F., Patanchon, G., Pearson, T. J., Perdereau, O., Perotto, L., Perrotta, F., Pettorino, V., Piacentini, F., Piat, M., Pierpaoli, E., Pietrobon, D., Plaszczyński, S., Pointecouteau, E., Polenta, G., Pratt, G. W., Prézéau, G., Prunet, S., Puget, J.-L., Rachen, J. P., Reinecke, M., Remazeilles, M., Renault, C., Renzi, A., Ristorcelli, I., Rocha, G., Rosset, C., Rossetti, M., Roudier, G., Rowan-Robinson, M., Rusholme, B., Sandri, M., Santos, D., Sauvé, A., Savelainen, M., Savini, G., Scott, D., Seiffert, M. D., Shellard, E. P. S., Spencer, L. D., Stolyarov, V., Stompor, R., Sudiwala, R., Sutton, D., Suur-Uski, A.-S., Sygnet, J.-F., Tauber, J. A., Terenzi, L., Toffolatti, L., Tomasi, M., Tristram, M., Tucci, M., Tuovinen, J., Valenziano, L., Valiviita, J., Van Tent, B., Vibert, L., Vielva, P., Villa, F., Wade, L. A., Wandelt, B. D., Watson, R., Wehus, I. K., Yvon, D., Zacchei, A., and Zonca, A., "Planck 2015 results - vii. high frequency instrument data processing: Time-ordered information and beams," *A&A* **594**, A7 (2016).

- ⁹¹C. L. Kuo, J. J. Bock, J. A. Bonetti, J. Brevik, G. Chattopadhyay, P. K. Day, S. Golwala, M. Kenyon, A. E. Lange, H. G. LeDuc, H. Nguyen, R. W. Ogburn, A. Orlando, A. Transgrud, A. Turner, G. Wang, and J. Zmuidzinas, “Antenna-coupled TES bolometer arrays for CMB polarimetry,” in *Millimeter and Submillimeter Detectors and Instrumentation for Astronomy IV*, Vol. 7020, edited by W. D. Duncan, W. S. Holland, S. Withington, and J. Zmuidzinas, International Society for Optics and Photonics (SPIE, 2008) pp. 415 – 428.
- ⁹²P. A. R. Ade, R. W. Aikin, D. Barkats, S. J. Benton, C. A. Bischoff, J. J. Bock, K. J. Bradford, J. A. Brevik, I. Buder, E. Bullock, C. D. Dowell, L. Duband, J. P. Filippini, S. Fliescher, S. R. Golwala, M. Halpern, M. Hasselfield, S. R. Hildebrandt, G. C. Hilton, H. Hui, K. D. Irwin, J. H. Kang, K. S. Karkare, J. P. Kaufman, B. G. Keating, S. Kefeli, S. A. Kernasovskiy, J. M. Kovac, C. L. Kuo, E. M. Leitch, M. Lueker, K. G. Megerian, C. B. Netterfield, H. T. Nguyen, R. O’Brien, R. W. O. IV, A. Orlando, C. Pryke, S. Richter, R. Schwarz, C. D. Sheehy, Z. K. Staniszewski, R. V. Sudiwala, G. P. Teply, K. Thompson, J. E. Tolan, A. D. Turner, A. G. Vieregg, A. C. Weber, C. L. Wong, and K. W. Y. and, “bicep2/KECK ARRAY. IV. OPTICAL CHARACTERIZATION AND PERFORMANCE OF THE bicep2 AND KECK ARRAY EXPERIMENTS,” *The Astrophysical Journal* **806**, 206 (2015).
- ⁹³K. Karatsu, A. Endo, J. Bueno, P. J. de Visser, R. Barends, D. J. Thoen, V. Murugesan, N. Tomita, and J. J. A. Baselmans, “Mitigation of cosmic ray effect on microwave kinetic inductance detector arrays,” *Applied Physics Letters* **114**, 032601 (2019), <https://doi.org/10.1063/1.5052419>.
- ⁹⁴A. D’Addabbo, M. Calvo, J. Goupy, A. Benoit, O. Bourrion, A. Catalano, J. F. Macias-Perez, and A. Monfardini, “High-energy interactions in kinetic inductance detectors arrays,” in *Millimeter, Submillimeter, and Far-Infrared Detectors and Instrumentation for Astronomy VIII*, Vol. 9153, edited by W. S. Holland and J. Zmuidzinas, International Society for Optics and Photonics (SPIE, 2014) pp. 883 – 895.
- ⁹⁵Planck Collaboration, Ade, P. A. R., Aghanim, N., Armitage-Caplan, C., Arnaud, M., Ashdown, M., Atrio-Barandela, F., Aumont, J., Baccigalupi, C., Banday, A. J., Barreiro, R. B., Battaner, E., Benabed, K., Benoit, A., Benoit-Lévy, A., Bernard, J.-P., Bersanelli, M., Bielewicz, P., Bobin, J., Bock, J. J., Bond, J. R., Borrill, J., Bouchet, F. R., Bridges, M., Bucher, M., Burigana, C., Cardoso, J.-F., Catalano, A., Challinor, A., Chamballu, A., Chiang, H. C., Chiang, L.-Y., Christensen, P. R., Church, S., Clements, D. L., Colombi, S., Colombo, L. P. L., Couchot, F., Coulais, A., Crill, B. P., Curto, A., Cuttaia, F., Danese, L., Davies, R. D., de Bernardis, P., de Rosa, A., de Zotti, G., Delabrouille, J., Delouis, J.-M., Désert, F.-X., Diego, J. M., Dole, H., Donzelli, S., Doré, O., Douspis, M., Dupac, X., Efstathiou, G., Enßlin, T. A., Eriksen, H. K., Finelli, F., Forni, O., Frailis, M., Franceschi, E., Galeotta, S., Ganga, K., Giard, M., Girard, D., Giraud-Héraud, Y., González-Nuevo, J., Górski, K. M., Grattton, S., Gregorio, A., Gruppuso, A., Hansen, F. K., Hanson, D., Harrison, D., Henrot-Versillé, S., Hernández-Monteagudo, C., Herranz, D., Hildebrandt, S. R., Hivon, E., Hobson, M., Holmes, W. A., Hornstrup, A., Hovest, W., Huppenberger, K. M., Jaffe, A. H., Jaffe, T. R., Jones, W. C., Juvela, M., Keihänen, E., Keskitalo, R., Kisner, T. S., Kneissl, R., Knoche, J., Knox, L., Kunz, M., Kurki-Suonio, H., Lagache, G., Lamarre, J.-M., Lasenby, A., Laureijs, R. J., Lawrence, C. R., Leonardi, R., Leroy, C., Lesgourgues, J., Liguori, M., Lilje, P. B., Linden-Vørnle, M., López-Cañiego, M., Lubin, P. M., Macías-Pérez, J. F., Mandolesi, N., Maris, M., Marshall, D. J., Martin, P. G., Martínez-González, E., Masi, S., Massardi, M., Matarrese, S., Matthai, F., Mazzotta, P., McGehee, P., Melchiorri, A., Mendes, L., Mennella, A., Migliaccio, M., Miniussi, A., Mitra, S., Miville-Deschênes, M.-A., Moneti, A., Montier, L., Morgante, G., Mortlock, D., Mottet, S., Munshi, D., Murphy, J. A., Naselsky, P., Nati, F., Natoli, P., Netterfield, C. B., Nørgaard-Nielsen, H. U., Noviello, F., Novikov, D., Novikov, I., Osborne, S., Oxborrow, C. A., Paci, F., Pagano, L., Pajot, F., Paoletti, D., Pasian, F., Patanchon, G., Perdereau, O., Perotto, L., Perrotta, F., Piacentini, F., Piat, M., Pierpaoli, E., Pietrobon, D., Plaszczynski, S., Pointecouteau, E., Polenta, G., Ponthieu, N., Popa, L., Poutanen, T., Pratt, G. W., Prézeau, G., Prunet, S., Puget, J.-L., Rachen, J. P., Racine, B., Reinecke, M., Remazeilles, M., Renault, C., Ricciardi, S., Riller, T., Ristorcelli, I., Rocha, G., Rosset, C., Roudier, G., Rusholme, B., Sanselme, L., Santos, D., Sauvé, A., Savini, G., Scott, D., Shellard, E. P. S., Spencer, L. D., Starck, J.-L., Stolyarov, V., Stompor, R., Sudiwala, R., Sureau, F., Sutton, D., Suur-Uski, A.-S., Sygnet, J.-F., Tauber, J. A., Tavagnacco, D., Terenzi, L., Toffolatti, L., Tomasi, M., Tristram, M., Tucci, M., Umaga, G., Valenziano, L., Valiviita, J., Van Tent, B., Vielva, P., Villa, F., Vittorio, N., Wade, L. A., Wandelt, B. D., Yvon, D., Zaccari, A., and Zonca, A., “Planck 2013 results. x. hfi energetic particle effects: characterization, removal, and simulation,” *A&A* **571**, A10 (2014).
- ⁹⁶Catalano, A., Ade, P., Atik, Y., Benoit, A., Bréele, E., Bock, J. J., Camus, P., Chabot, M., Charra, M., Crill, B. P., Coron, N., Coulais, A., Désert, F.-X., Fauvet, L., Giraud-Héraud, Y., Guillaudin, O., Holmes, W., Jones, W. C., Lamarre, J.-M., Macías-Pérez, J., Martínez, M., Miniussi, A., Monfardini, A., Pajot, F., Patanchon, G., Pelissier, A., Piat, M., Puget, J.-L., Renault, C., Rosset, C., Santos, D., Sauvé, A., Spencer, L. D., and Sudiwala, R., “Impact of particles on the planck hfi detectors: Ground-based measurements and physical interpretation,” *A&A* **569**, A88 (2014).
- ⁹⁷R. A. Mewaldt, A. J. Davis, K. A. Lave, R. A. Leske, E. C. Stone, M. E. Wiedenbeck, W. R. Binns, E. R. Christian, A. C. Cummings, G. A. de Nolfo, M. H. Israel, A. W. Labrador, and T. T. von Rosenvinge, “RECORD-SETTING COSMIC-RAY INTENSITIES IN 2009 AND 2010,” *The Astrophysical Journal* **723**, L1–L6 (2010).